SYNTHESIS AND CHARACTERIZATION OF POLYMER COMPOSITES CONTAINING ALIGNED CONDUCTING POLYMERS AND CARBON NANOTUBES

A Thesis

by

SWATHI MANDA

Submitted to the Office of Graduate and Professional Studies of
Texas A&M University
in partial fulfillment of the requirements for the degree of

MASTER OF SCIENCE

Chair of Committee,	Choongho Yu
Committee Members,	Sy-Bor Wen
	Harlan Rusty Harris
Head of Department,	Andreas A. Polycarpou

May 2014

Major Subject: Mechanical Engineering

ABSTRACT

Miniaturization of electronics and impending demand for bendable electronic gadgets creates a dire need for a thin and flexible film technology that would not only provide spot cooling for the crammed transistors, but also tap into the waste heat generated to produce a portable power source. Thin film thermoelectrics offer a viable solution and have several structural, chemical and economical advantages over inorganic thermoelectric materials. However, their low power factor compared to that of inorganic materials prevents them from being used for practical applications. The tradeoff between Seebeck coefficient and electrical conductivity restricts the improvement of power factor through increase in number of charge carriers. However, controlled modulation of the mobility of charge carriers has a potential to increase the electrical conductivity without adversely affecting the Seebeck coefficient. This research involves investigating a novel way to fabricate organic thermoelectric thin films with high power factor by modulating the morphology of the conducting polymer poly-(3,4-ethylenedioxythiophene) (PEDOT) and creating a composite with carbon nanotubes to control the mobility and hence the electrical conductivity of the thin films. Aligned PEDOT-carbon nanotube composite thin films were fabricated and characterized to study both the alignment of the polymer chains and change in their electrical conductivity.

This research utilized the bottom up self organized molecular system templates to control the nano structure and ordering of the polymer–carbon nanotube composite.

Liquid crystal template was used to capture all the monomer (3,4-ethylenedioxythiophene) EDOT molecules within the cylindrical cores of hexagonal mesophase oriented in effective net direction within domains, and the monomers were electro-polymerized to obtain aligned polymer chains. This aligned structure renders better anisotropic electrical conductivity along the polymer chain direction. A non percolated dispersion of carbon nanotubes and dopants was incorporated into the aligned PEDOT thin film by spraying as well as internally dispersing within the liquid crystal network before polymerization. The carbon nanotube and dopant incorporation into the aligned PEDOT thin films increased the electrical conductivity by about two orders of magnitude.

DEDICATION

Dedicated to my Grandfather and Grandmother,

without whose selfless love and support I would not have come so far.

ACKNOWLEDGEMENTS

First, I gratefully acknowledge my advisor, Dr. Choongho Yu, for his motivation, challenges and guidance throughout the entire period of my research. This research would not have been successful without his constant mentoring and encouragement and I am thankful to him for giving me the great opportunity to work and learn in this exciting field of research. I also thank my committee members, Dr. Rusty Harris, and Dr. Sy-Bor Wen, for their invaluable advice and feedback.

I also extend special thanks to my colleague Jui-Hung Sue whose guidance and support was pivotal in completing this research. I thank all my colleagues at the Nano-energy lab: Dr. Hong Wang, Abdullah Tazebay, Dr. Kyungwho Choi, Xiong Pu, Dr. Liang Yin, Suk Lae Kim, Woongchul Choi, Dr. Sang Won Jee, Su-In Yi and Gang Yang for their constant help and encouragement. I also express my deep appreciation to Dr. James Hulvat from the Stupp Laboratory at Northwestern University, whose unhesitant prompt clarifications and guidance helped me to overcome crucial bottlenecks in my research.

I extend my sincere thanks to my parents and family for their unconditional love and support. Without their encouragement, it would have been impossible for me to have a research career.

I appreciate the friendship and support of my friends Lian Ma, Kelly Guiberteau, Ramy Moaness Saleh, Nafiz Chowdary, Priyam Parikh and many others who have made my

experience at Texas A&M University a memorable one. Last but not the least, I am grateful to my friends from IIT Jodhpur whose constant inspiration and support was invaluable throughout my study.

TABLE OF CONTENTS

Page

LIST OF FIGURES

Page

LIST OF TABLES

Page

NOMENCLATURE

2-D	2-Dimensional
3-D	3-Dimensional
Ag	Silver
Au	Gold
Bi	Bismuth
CNTs	Carbon nanotubes
CSA	Camphorsulphonic acid
CV	Cyclic voltammetry
DI	De-ionized
DMSO	Dimethylsulphoxide
EDOT	(3, 4-ethylenedioxythiophene)
$(EO)_{10}$-oleyl	Poly $(oxyethylene)_{10}$-olyel ether
$FeCl_3$	Iron (III) Chloride
FET	Field effect transistor
Ge	Germanium
HOMO	Highest occupied molecular orbital
I-V	Current vs. Voltage
κ	Total thermal conductivity
κ_e	Electronic contribution of thermal conductivity
L	Length

LC	Liquid Crystal
LED	Light emitting diode
LUMO	Lowest unoccupied molecular orbital
M	Molar
μ	Mobility of charge carriers
n	Number of charge carriers
nm	Nanometer
PAA	Polyacrylic acid
PDMS	Polydimethylsiloxane
PEDOT	Poly (3, 4-ethylenedioxythiophene)
Π	Peltier coefficient
POM	Polarized optical microscope
PSS	Poly (sodium styrene sulphonate)
PTFE	Polytetrafluoroethylene
PV	Photovoltaic
ρ	Electrical resistivity
rpm	Rotations per minute
S	Seebeck coefficient
SAM	Self assembled monolayer
Scm^{-1}	Siemens per centimeter
SDBS	Sodium Dodecylbenzenesulphnate
Se	Selenium

SEM	Scanning electron microscope
σ	Electrical conductivity
Si	Silicon
Sm^{-1}	Siemens per meter
t	Thickness
T	Absolute temperature
ΔT	Temperature difference
Te	Tellurium
TE	Thermoelectric
TEAP	Tetraethylammonium perchlorate
TEG	Thermoelectric generator
T_i	Isotropization point
ΔV	Voltage difference
W	Width
ZT	Thermoelectric figure of merit

1. MOTIVATION AND INTRODUCTION

The world's first electronic computer called ENIAC, which was built in 1946 and weighed about 30 tons, used nearly 19,000 vacuum tubes that had to be cooled using an array of fans to keep them from burning.[1] As time progressed, the advent of solid-state Silicon (*Si*) technology, and the more recent shift from 'bipolar' transistor technology to complementary metal oxide semiconductor devices, offered some respite in terms of electronic cooling by drastically reducing the energy dissipated per device. However, the escalating computing power of the micro-devices roughly doubles every 18 months, as famously observed by Moore's law, and demands the exploration of powerful and efficient cooling technologies to prevent the components from melting. Furthermore, the heat radiation from everyday electronics like laptops and cellular phones poses a serious threat to the human body. The heat flux generated by these devices is loosely in the league of sun's heat flux.[2] Recently, a condition known as *Erythema ab igne*, or otherwise "Toasted skin syndrome" has been reported in a young individual due to constant laptop heat radiation reaching 50˚ Celsius (˚*C*).[3] The more the microelectronics shrink, the hotter they get and more is the need for effective cooling which can complement the efficient performance of transistors.

Several new technologies are being explored for the fundamental thermal energy management problem in computing. Liquid coolants are being pumped directly onto the chips rather than circulating air around them and 3-D packaging of circuitry is being

investigated for effective heat transfer passages by using heat sinks. But cooling an advanced computer at a facility like Leibniz Supercomputing Center in Munich, which can operate at nearly 3 petaflops, would need several cubic kilometers of air everyday and this heat can even amount to warming some of the centre's buildings directly.[2] More recently, waste heat recovery systems that are based on solid state thermoelectric materials are gaining prominence. Thermoelectrics (TE) not only absorb the low grade waste heat, but they can also utilize the temperature difference to generate voltage, thereby promising a secondary source of power. Green devices based on the conventional thermoelectric materials like Germanium (*Ge*) and Tellurium (*Te*) that can cool and regenerate power hold a huge potential in the electronic cooling industry.

The turn of the millennium witnessed the need for flexible electronic materials for a variety of applications. This need was partially addressed by cramming a huge number of miniaturized standard Si-chip based microelectronics into a flexible substrate. But, this miniaturization of inorganic semiconductors is not feasible for applications that spread over a wider area like the more recent Organic LEDs and Organic Photovoltaics. With Si, one would need a large number of embedded chips to achieve uniform intensity and performance, but that would again lead to high heat generation which can possibly melt off the flexible substrate. Instead the focus is now shifting to bendable electronics made of intrinsically conductive and flexible thermoelectric materials, which have slightly lower performance, spread over a large area and bring down the temperatures. Also, the flexible TEs double as micro power generators by using the dissipated heat to

generate back voltage, which is very attractive for a wide range of biological and chemical sensory applications.

The numerous applications and advantages of the organic TEs demand for high efficiencies of power conversion for practical use. This research focuses on investigating the fabrication of such a novel, flexible thermoelectric thin film, with a comparable performance, which could find applications in the bendable electronic industry by offering a flexible substrate alternative which could also efficiently take care of the thermal dissipation problem. This chapter gives a brief background and motivation into why the bottom up fabrication technique was adopted and offers a rationale for choosing the organic polymer as a base to the thin film rather than more traditional inorganic thermoelectric materials.

The sea change and sophistication in the electronic industry demand for more versatile "nano" components that can be mass produced, decrease the cost commercially, pack components in more densely and improve the performance of the devices. The future of the communication industry demands ultra thin wearable, bendable and disposable electronics based on cheap and heavy performing nano electronics. The two most commonly used nano fabrication techniques in the electronic industry today are the top-down approach and the bottom-up approach. The conventional top-down approach generally involves gradual material removal using lithography or micro-machining techniques and can fabricate ultra small structures with high accuracy and repeatability.

But it involves large investments, operating costs, limited application in terms of materials, non eco-friendly chemicals, and demanding clean room environments. Additionally, even the latest conventional lithographic techniques, such as focused ion beam technology for fabricating quantum sized features, are restricted to only 2-D planes.[4] Though the ubiquitous silicon is the most popular and widely used material in the semiconductor industry, the inorganic materials have several limitations when we consider applications involving transparent, bendable, light weight and disposable electronics. As the characteristic length scales shrink and hit tens of nanometers (*nm*), the serial top-down approach faces serious limitations in terms of scalability and accuracy of small features.

On the other hand, bottom-up manufacturing approach can routinely produce extremely small and complex nanostructures as small as 1 *nm*. This approach utilizes the bonds and interactions at the molecular level to form an assembly of desired nanostructures in a wide variety of materials including conventional silicon as well as organic polymers. The main advantages to the bottom- up approach are three fold: first, it is faster, more environmental friendly, relatively simple and cost effective. Second, it provides an added advantage of 3-D structural control which is very important for manufacturing arbitrary patterns, influencing properties precisely and for introducing site-specific functionality into the structures. Third, with the emergence of organic material alternatives, one can take advantage of molecular tuning to control the bulk properties like luminescence, electrical conductivity, strength, etc. Though this approach is still

being investigated for accuracy and repeatability, processes like self- assembled monolayers (SAMs) and dip pen lithography are gaining rapid importance in applications like manufacturing of Organic FETs, thermoelectric composites, etc.

Conductive organic materials offer a viable alternative to traditional inorganic semiconductors like Si and Ge. Though the organic materials offer a relatively low mobility of charge carriers and cannot rival the high performance of highly-ordered single-crystalline materials, they offer several advantages:

1. The inherent unique structural flexibility of organic materials offers a niche application for novel thin film electronics like organic electronic paper, smart cards, bendable phone displays, rollable electronic watches, etc.
2. Low-energy, low-cost, high-yield and accessible processing techniques such as solution processing, spin coating, direct printing and evaporation, eliminate the need for high vacuum or high temperatures. This ushers in a whole new dimension of applications involving plastic substrates, which was not achievable previously due to the high temperatures of over 900˚ C required in Si lithography.
3. Lower performance leveraged with a decrease in cost opens a new window for creating new consumer habits of replaceable and disposable everyday electronics such as electronic luggage tags, bionic e-skins[5], e-textiles, large cheap interchangeable displays, low cost memory devices, etc.

4. Specific controllability of properties using bottom-up fabrication techniques such as self-assembly offers the possibility of surpassing the current performance challenged by inorganic materials in particular applications.

Since their evolution in 1975, conductive polymers are one exciting class of organic materials that are extensively being invested in for research as they offer a great application potential. Traditional polymers are generally insulating, but if electrical conductivity is possible, for example in the case of conjugated polymers like poly-aniline and poly-ethoxydithiophene, they are an extremely attractive alternative to inorganic conductors and semi-conductors because of their physical and chemical properties such as high strength to weight ratio, toughness, reduced processing cost, ease of fabricating complex structures and controllability of molecular structure. Their conducting or semi conducting properties, along with their low thermal conductivity make them feasible for applications in organic light emitting diodes, photovoltaics[6] and more recently, thermoelectric devices.

Traditional inorganic semi-conductor materials like Bismuth (*Bi*), *Te* and Selenium (*Se*) deliver high thermoelectric power and deliver nearly four times more efficient energy conversion than the organic materials. But, because of the diverse and unique material properties as discussed above, the inclusion of conducting polymers to form complementary hybrids is being extensively explored. However, the organic conducting polymers exhibit lower mobility and lower electrical conductivity (σ nearly 0.1 – 100

Scm^{-1}) than the inorganic thermoelectric counterparts (σ > 1000 Scm^{-1}), rendering them inefficient for independent practical conversion applications.[7] Thus, there exists a dire need for enhancing the electrical conductivity of organic conducting polymers to make them commercially viable for a plethora of applications.

This research focuses on investigating a novel method to fabricate organic conducting polymer based thermoelectric thin-film composite with high power factor. Since the properties of organic conducting polymers are dominantly affected by the molecular arrangement, designing and controlling the supra molecular ordering of these molecules at the nano and meso scales provides a facile route for enhancing the bulk properties such as electrical conductivity and thermoelectric performance. This research utilizes self-assembled molecular system templates to control the ordering and orientation of the polymer chains. The effect of deliberately dispersing short carbon nanotube fibers in a non-percolated fashion inside the ordered polymer matrix is investigated for enhancement of bulk electrical conductivity. Through this method, thin films of organic material composite with enhanced thermoelectric power factor can be fabricated owing to the controlled orientation arising from molecular ordering.

2. LITERATURE REVIEW

2.1 Thermoelectric Materials

Thermoelectric (TE) materials transform heat flow into electric voltage or vice versa, i.e. electricity into temperature difference.[8] The conventional methods of converting thermal energy into electricity include the thermodynamic heat cycles such as Rankine cycles, which involve complex rotor equipments, high heat losses and impact the environment negatively due to production of green house gases.[9] On the other hand, TE energy conversion is mechanically robust as it uses solid state technology that does not involve any moving parts, and is environmentally safe. TE energy conversion systems are quiet, compact, reliable, and maintenance free.[8, 10, 11] With the increasing global demand for energy sources that are affordable, green as well as sustainable, TE materials are gaining prominence over the fossil fuels owing to the clean energy they can generate from a variety of sources including the abundant solar energy, geothermal sources, low grade waste heat from automobiles and electronic equipments.

TEs can function either as thermoelectric generators (TEG) or Peltier coolers.[8] TEGs collect the thermal energy whenever there is a temperature gradient and transform it into potential difference across the ends, while the Peltier Coolers generate a cooling effect on one end of the material by consuming electric energy. Their functioning can be explained basing on the two fundamental phenomena occurring in TEs.

2.1.1 Seebeck effect

In 1800's Seebeck discovered that when there is a temperature difference (ΔT) created between the two end joints of 2 dissimilar materials held together, a voltage difference (ΔV) that is proportional to ΔT is developed.[8] The ratio of the voltage developed from a given temperature gradient ($\Delta V/\Delta T$) is a function of the intrinsic property of the material called the Seebeck coefficient (S).

$$S = \frac{\Delta V}{\Delta T}$$

All the materials exhibit some Seebeck effect, but for practical application purposes, it is of a measurable magnitude only in some materials and these are called TE materials. The Seebeck effect is extremely low for metals (only a few $\mu V/K$) while it is much larger for semiconductors (typically a few hundred $\mu V/K$).[12] The functioning of a TEG can be described by the Seebeck effect. A typical thermoelectric cycle involved the charge carriers i.e. electrons as the working fluid and follows the fundamental laws of thermodynamics closely resembling the Carnot heat engine cycle. Fig. 2.1 shows the schematic of the operation of a TEG based on Seebeck effect. The heat source or the hot junction is maintained at a temperature T_H and heat is constantly pumped at the rate Q_H while the cold junction maintained at a temperature T_L rejects the heat at a constant rate Q_L . It should be noted that the output electric power ($\dot{We}$) generated from a TEG depends on the difference between the input and output heat transfer rates as energy is conserved.

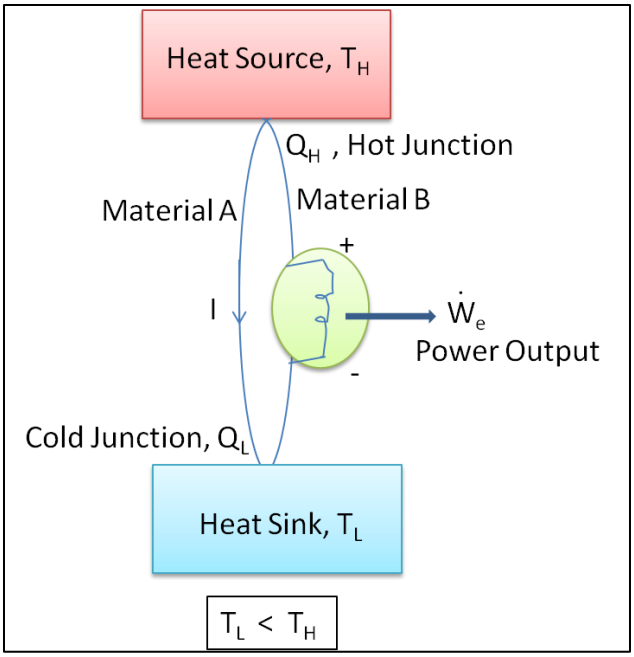

Fig. 2.1: Operating principle of a TEG based on the Seebeck effect.

The major deficiency in TEG devices for extensive applications is their low efficiency of power conversion which is typically about 5%.[13] Thus, so far, they have been restricted to niche applications like portable and remote power generation, or heat based sensing in military, medical, industrial, and aerospace fields where the primary requirement is high reliability without a restriction on the cost.[8, 13, 14] However, in the recent times, with the increasing awareness and concern for alternative green sources of power, and the abundance of the sensible heat that dissipates into the environment increasing the green house effect, TEGs have received importance in large scale applications. TEGs offer a facile route to convert the low grade waste heat (typically <200˚ *C*) that cannot be captured using the conventional power generators into electric power. Since the conversion of even a fraction of the waste heat into electric power is advantageous, the

low conversion efficiency of TEG no longer imposes a critical drawback and the cost of the input energy becomes redundant factor.[8, 15] Few examples include cogeneration systems[16], automobile engine waste heat radiation[17], industrial pipelines carrying hot effluents, etc.

2.1.2 Peltier effect

Peltier observed that when electric energy is passed through two dissimilar materials joined together, heat energy is either generated or absorbed at the junctions, based on the direction of flow of the current.[18] This is called Peltier effect and the main cause of this phenomenon is the difference in the Fermi energy levels of the two materials. Peltier coefficient Π, is defined as:

$$\Pi = ST$$

Thus Peltier and Seebeck effects are related to each other. The rate of liberation of heat at the hot junction Q_P is given by:

$$Q_P = \frac{S}{T}$$

The Peltier effect is the basis for several TE refrigeration applications. An example includes the small localized spot cooling for computers, optoelectronics, infrared detectors, etc. These devices do not impose a heavy heat load and effectively maintaining them at optimal temperatures has the potential to increase their performance. Especially, in the field of computing, cooling the processors can produce

computing speed gains of 30-200%.[19] Fig. 2.2 shows a typical functioning of a Peltier cooler.

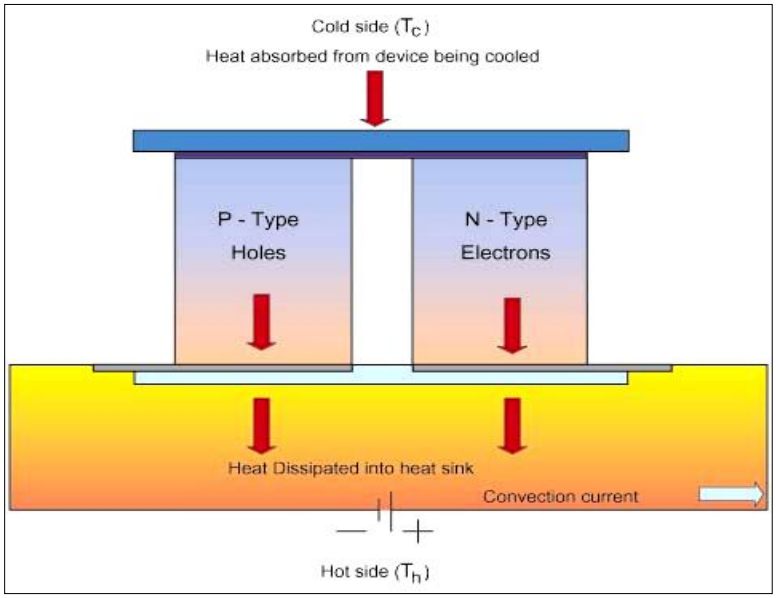

Fig. 2.2: Schematic of Peltier effect based TE cooler.[20]

Some versatile thermoelectric modules can function as both TEG and Peltier Coolers. They consist of both p-type (heavily doped to create excess holes) and n-type (heavily doped to create excess electrons) semiconductors suited to operate according to the input conditions.

2.1.3 Thermoelectric figure of merit

The potential of performance of a material for TE applications is mainly determined by its thermoelectric figure of merit (*ZT*), which is a dimensionless quantity defined as:

$$ZT = \frac{S^2.\sigma.T}{\kappa} = \frac{S^2.T}{\rho.\kappa}$$

where S is the Seebeck coefficient, σ is the electrical conductivity, ρ is the electrical resistivity, κ is the total thermal conductivity and T is the absolute temperature. The numerator in the above expression, $(S^2.\sigma.T)$ is called the power factor. Currently, the state of the art TE materials such as Bismuth Telluride based alloys and Lead Telluride based alloys possess a *ZT* value around 1 (Fig. 2.3) [21], with an efficiency of cooling or power generation around 10-30% of that of conventional thermal engines. Recent materials that exhibit *ZT* > 1 are expected to compete against more conventional of refrigeration and electric power generation.[22-24]Several different classes of materials have been studied for TE applications, including conducting oxides such as clathrates, skutterudites, metal alloys such as half-Heusler alloys, and pentatellurides. [25] In fact, Bismuth Telluride alloys have been shown to exhibit the best TE efficiencies till date. Materials that exhibit *ZT* nearly 2 have been observed to possess very low lattice thermal conductivities.[22, 23] Fig. 2.3 illustrates schematically the *Z* values as a function of $\bar{T}(℃)$ for some conventional TE materials.[26] However, many of the above classes of materials are toxic and *Te* is one of the rarest elements on earth. Thus the production of these alloys on a large scale involves several problems such as high cost of production, toxicity and unavailability.

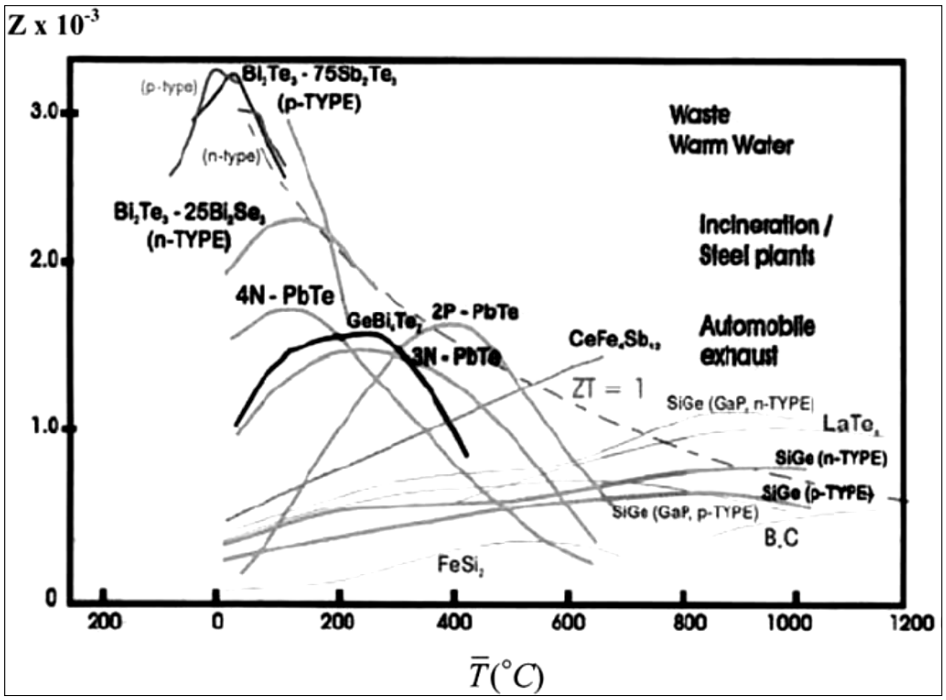

Fig. 2.3: Z values with respect to $\overline{T}$(℃) plotted in comparison to ZT = 1 (hashed line) for a number of conventional state of the art TE materials and their applications.[26]

2.1.4 Relationship between the thermoelectric properties and relationship with thermo-power

Highly effective TE materials should possess higher ZT values. Most of the current day research in TE materials is focused on either finding new TE composites that can operate at broader and high temperature ranges (T< 250K and T>400K) or improving the ZT by improving the intrinsic TE nature of the material. ZT value can be maximized by achieving high electrical conductivity (σ) and high Seebeck (S) values while decreasing thermal conductivity (κ), especially through manipulation of the nanostructure at the molecular level.

It is desirable to tune a TE material to achieve high S and σ values simultaneously to increase the power factor. However, in conductors and heavily doped semiconductors, there is a limitation in improving the S and σ values because they are tied to each other through the Mott relationship, and the ratio is essentially constant at a given T.[27] Fig. 2.4 shows the schematic of the relation between S and σ values as a function of the carrier concentration at a given temperature for different categories of materials.[28] The following equation demonstrates the actual correlation between them through the common factor of number of charge carriers (n):

$$S = \frac{\pi^2 k^2 m^* T}{(3\pi^2)^{2/3} \hbar |e| n^{2/3}}$$

Electrical conductivity can be described as a function of the charge carrier concentration (n) and carrier mobility (μ) as dictated by the following equation:

$$\sigma = n.\ e.\ \mu$$

Also the Wiedemann–Franz Law ties together the electrical conductivity and electronic contribution of thermal conductivity in conductors through the following relation, which simultaneously increases κ_e with any increase in σ:

$$\kappa_e/\sigma = L.\ T\ ,$$ where the constant $L = 2.44 \times 10^{-8}\ W\Omega K^{-2}$

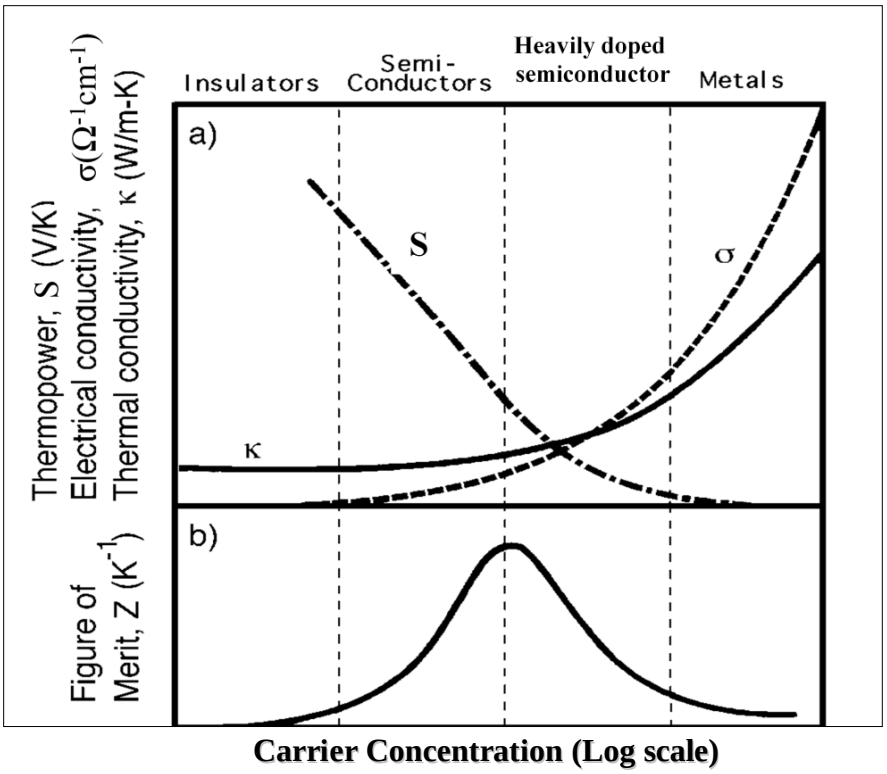

Fig. 2.4: Relationship between σ and S for different carrier concentrations at a given T.[28]

To achieve highest conversion efficiency, it is important to have high ZT, which requires that the highest electrical conductivity for a given carrier concentration be achieved. Generally, σ and thereby the power factor are optimized in narrow-gap semiconducting materials as a function of carrier concentration (typically about 10^{19} carriers/cm^3), through doping (usually highly conducting materials such as metal nanoparticles and carbon nanotubes (CNTs)), to result in the largest ZT.[23] But, since the thermal and electrical conductivity correlate with the charge carriers, a new perspective must be introduced in order to conciliate the contradiction between high σ and low κ.[24] Increasing the mobility of the carriers is another way to increase σ and power factor without affecting S and κ.

2.2 Organic Thermoelectrics

High *ZT* values exhibited by the inorganic TE materials alone are not sufficient for creating a viable technology platform for practical applications. They should also be easily synthesized, stable, environmentally friendly and solution processable to create patterns on large areas. Because of the several disadvantages associated with the manufacturing of inorganic TE materials and the limited applications due to their rigid nature, organic thermoelectric materials have gained importance.

The fundamental property TE materials should possess is that they must be good conductors of electricity but not heat. That way, due to the virtue of low thermal conductivity, one end of the material can get hot while the other end can remain cold and thus provide the temperature difference instead of quickly equalizing the temperature. In most inorganic conductors and semi-conductors, electrical and thermal conductivities go hand in hand. Thus they impose a challenge in creating highly efficient TE materials.

On the other hand, most organic thermoelectric materials are inherently poor thermal conductors ($\kappa \sim 0.2 Wm^{-1}K^{-1}$).[29, 30] Thus they immediately satisfy one important criteria of creating a good TE material. As far as possessing good electrical conductivity, a special class of organic materials called the conducting polymers have shown promising potential since the initial discovery of doped Poly-acetylene around late 1970's. In general, polymers exhibit poor electrical conductivity, but conjugated polymers that

have been doped with highly conducting particles exhibit semiconducting properties. Such organic conducting polymers have found several applications in solar cells[31-33], light emitting diodes(LEDs)[34, 35], transistors[36, 37], chemical and bio sensors[38], etc. Some examples of conjugated semi-conducting polymers that have found practical thermoelectric applications are Polyacetylene[39, 40], Polypyrroles[41, 42], Polyanilines[42-44], Polythiophenes[45, 46] , Poly(2,7-carbazole)s[47], etc (Fig. 2.5).

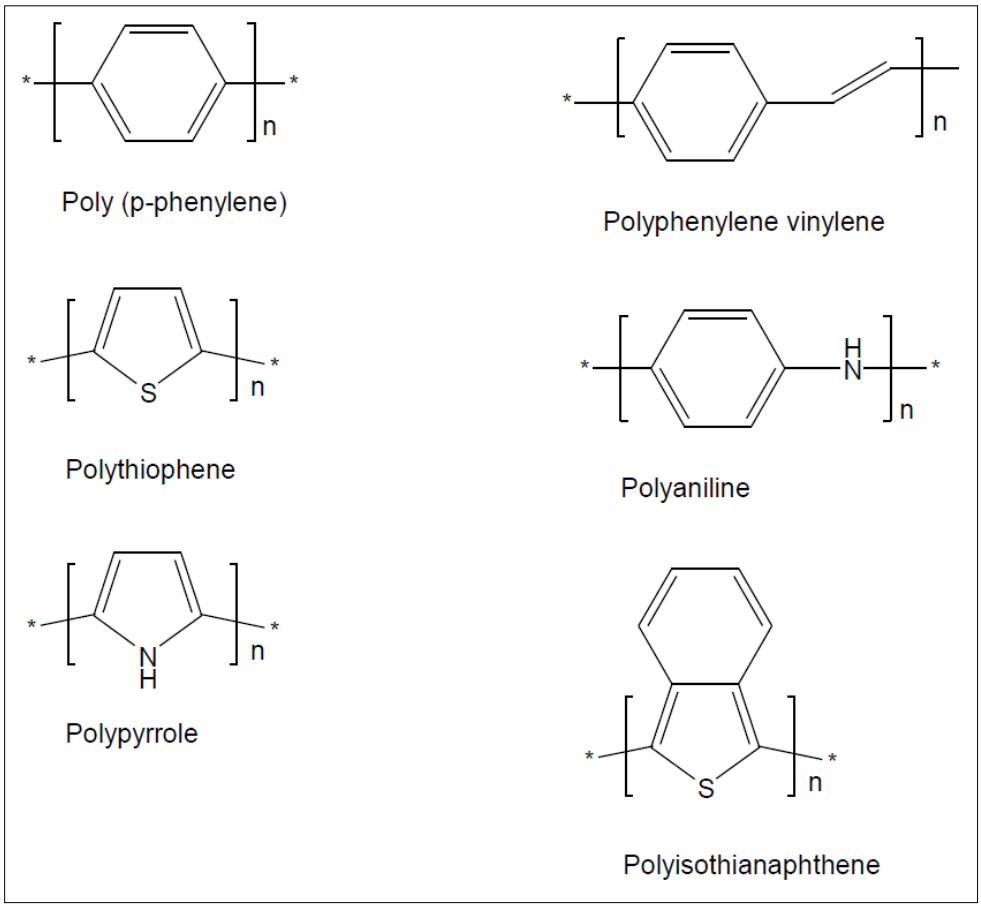

Fig. 2.5: Chemical structures of commonly used conducting polymers[48]

2.2.1 Theory of electrical conduction in conjugated polymers

The molecular origin of the electrical conductivity in the conducting polymers can be explained through the band theory as associated with the quantum theory and the molecular orbital theory. The physical chemistry approach to band theory through quantum mechanics states that atoms can occupy only specific and well defined energy levels.[49] For isolated atoms, these states are very sharp and distinct. The spectral emission lines of narrow width associated with each electron jump from one state to another stand a testimony to the distinct energy levels.[49] However, in a crystalline solid, the atoms are no longer isolated and see each other's electric fields, and hence the atomic energy states broaden into band like energy states within the crystal. This is demonstrated by a simple schematic of the 3s and 3p orbital of the metallic atom in the 3rd period of the periodic table (Fig. 2.6).[50] The chemical approach, on the other hand, dictates that when atoms are in close proximity, their atomic molecular orbitals overlap with each other resulting in the formation of molecular orbitals called the bonding orbital or the valence band (σ orbital with energy lower than the atomic orbitals) and the antibonding orbital or the conduction band (σ^* orbital with energy higher than the atomic orbitals).[50] The energy band gap between these delocalized molecular orbitals is called the band width and denotes the energy gap between HOMO (highest occupied molecular orbital, i.e. the valence band) and LUMO (lowest unoccupied molecular orbital, i.e. the conduction band) levels (Fig. 2.7).

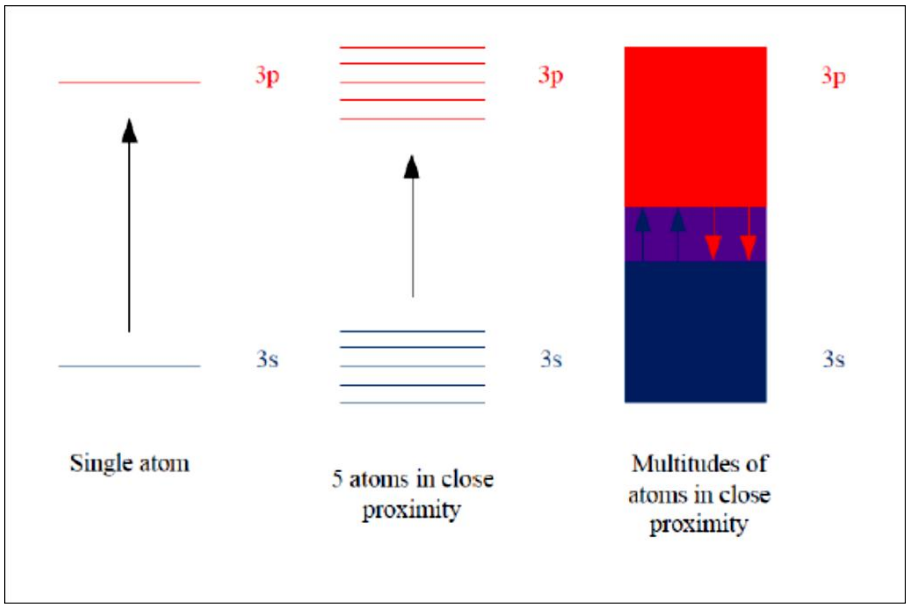

Fig. 2.6: Formation of band structure in the third period showing an overlap between the valence and conduction bands.[50]

In most of the traditional polymers such as polyethylene, the valence electrons are bound to sp^3 hybridized molecules with covalent bonds. Since these electrons lie in the stable sigma bonds, they have low mobility and hence they do not contribute to the electrical conductivity of the material. For a polymer to be conducting, it has to have a conjugated backbone molecular arrangement.[51] Their backbones contain sp^2 hybridized C atoms, where one electron resides in the p_z orbital, which is orthogonal to the plane of 3 other hybridized σ bonds. All such p_z orbitals that are in close proximity to each other combine to give rise to a delocalized set of orbitals that reside over the whole molecule. The extent of such delocalization and the alternation of the double and single bonds within the conjugated backbone of the polymer dictate the band width of the material, and

hence influence the electrical conductivity. Fig. 2.8 shows the influence of band width on the electrical conduction properties of metals, semiconductors and insulators.

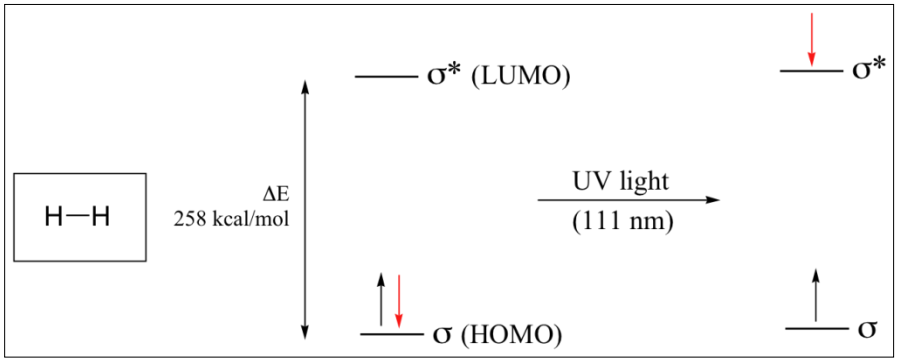

Fig. 2.7: Energy band gap between the molecular orbitals in a diatomic molecule.[52]

The presence of delocalized *Π* orbitals in the conjugated polymer chain alone is not sufficient to render them electrically conductive. Undoped conjugated polymers usually exhibit insulating or semiconducting property where the band gap is greater than 2 *eV*, which is too large for thermally activated conduction. Hence, undoped conjugated polymers, such as polythiophenes and polyacetylenes have a low electrical conductivity of around 10^{-10} to 10^{-8} *S/cm.*

There are three ways in which a material can be made electrically conducting:

1. Conduction within the same band: This occurs when the valence band of the material is not completely filled. In this case, the electron can excite to an energy level within the valence band itself, and hence can detach from its atom.[53] Since

the gap for excitation is small, many electrons can achieve this even with a small amount of energy.

2. Small band gap: When the band width between the valence and conduction bands is small, the electrons can absorb energy and excite to a higher band and thus get detached from their atoms. These electrons in the conduction band, as well as holes formed due to loss of electrons in the valence band, both contribute to the electrical conductivity.
3. Doping: This is a process of adding external impurity element of either higher or lower valency into the material to create an excess of electrons or excess of holes. Thus more the number of charge carriers, more the delocalization of orbitals over the molecule, lower the band width and higher the electrical conductivity.

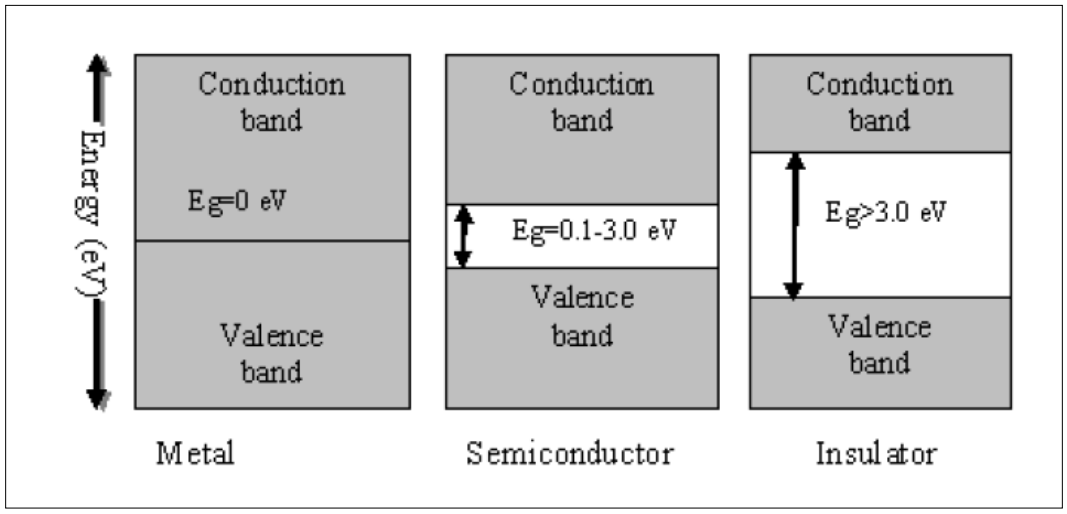

Fig. 2.8: Schematic showing band width in metals, semiconductors and insulators.[48]

To make the conjugated polymer electrically conductive, it is usually doped through oxidation. This process removes some of the delocalized electrons in the molecular *p* orbitals, and hence it creates a high mobility for the remaining electrons. The conjugated orbitals form a directional electronic cloud and these electrons become highly mobile when they are partially removed. This process creates a p-type conducting polymer. Similar process can be used to create an n-type conducting polymer through reduction by pumping excess of electrons into the unfilled delocalized orbital. It has been observed that even a low level of doping (i.e. less that 1%) in conducting polymers can give rise to improvement of several orders of magnitude of the electrical conductivity, even of values up to 0.1 *S/cm* and higher.[54]

2.2.2 PEDOT: Promising organic TE material

Poly(3,4-ethylenedioxythiophene) (PEDOT) is a conjugated polymer derivative of polythiophene. It stands out in the industry from other conducting polymers due to its remarkable properties of electrical conduction, high transparency, ease of processing and stability. Furthermore, PEDOT is amongst the conducting polymers which have gained popularity as commercially viable materials.[55] Its widespread applications include solid electrolyte capacitors[56] and more popularly light emitting diodes (LEDs) [57], organic PVs and organic field effect transistors (FETs) [58].

PEDOT is prepared by oxidative chemical method or electro-polymerization of the monomer ethylenedioxythiophene (EDOT) (Fig. 2.9) and unlike most aromatic linear

molecules is highly insoluble in organic solvents. To render it soluble, often side chains need to be incorporated into 3rd or 4th position.

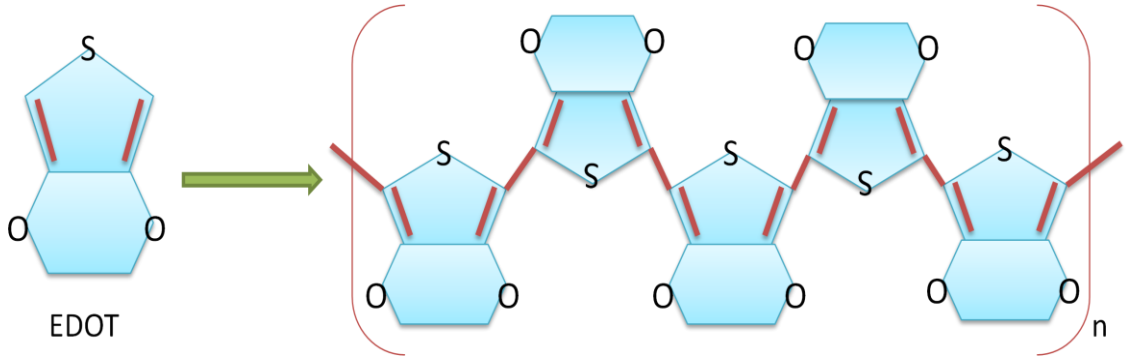

Fig. 2.9: Formation of conjugated backbone of PEDOT from monomer EDOT.

PEDOT exhibits high electrical conductivity of about 300 *S/cm*, but this often varies depending on the method of preparation used.[55] For practical applications, PEDOT is often doped with poly (styrene sulphonic) acid (PSS), which not only renders solubility to PEDOT, but also induces more charge carriers thereby rendering film formation ability, high transmissivity of visible light and stability to the material while still maintaining a good electrical conductivity of about 10 *S/cm* the electrical conductivity.[59] When the polymer anion PSS was replaced by smaller tosylate anion, the electrical conductivity improved to over 1000 *S/cm*, and yielded a *ZT* value 0.25 at room temperature, which is the highest performance bar so far amongst the organic thermoelectric materials.[60] Hence, PEDOT offers a great potential for tuning the molecular structure to improve the thermoelectric properties even further.

2.2.3 Routes to creating better thermoelectric properties for organic thin film electronic applications

Though the inorganic materials have a direct relationship between σ and S through the charge carrier concentration, the relationship between σ and S are not very well understood in case of organic thermoelectric materials. However, it has been identified that there exists a correlation between morphology, chain structure and electrical conductivity. It is assumed that the conductivity is higher for more crystalline structures and better aligned chains. At the same time, addition of nano structures into the polymer complex reduces the transmission of phononic vibrations reducing the κ values and hence improving the *ZT* value. Furthermore, adding dopants or counterions increases the number of charge carriers and hence is shown to greatly improve σ. However, indefinitely increasing the number of the charge carriers is not found to improve σ. Beyond a certain limit, the increase in *n* adversely affects the *ZT* value due to observed decrease in *S*.

2.3 Liquid Crystal Templating of Conducting Polymer

A typical way to produce conformal thin TE films on arbitrary geometries is through the process of electro-polymerization. Though this is a convenient technique, the films formed are usually amorphous with a number of structural defects. The defects affect the σ of poly-thiophene thin films. The σ of poly-thiophene has some dependence on the conjugation of the polymer backbone. To obtain maximum conjugation, poly-thiophene

must be coupled α - α' in regioregular manner. This configuration facilitates π orbital overlap and provides maximum conjugation with highly delocalized electronic cloud due to the planar aromatic backbone. S atom's lone pair of electrons play a major part in deprotonating the α carbon and thus facilitate α - α' coupling.[61] Though this structure is highly desirable, it is not always obtained during electro-polymerization because of the disruptions and formation of α-β' and other bonds due to highly energetic states. One method to decrease these defects is to use substituted monomers such as EDOT. This method blocks the β sites and reduces the defect formation.

To obtain effective TE performance, it is necessary to reduce the above structural and electronic defects during the formation of PEDOT from electro-polymerization of EDOT monomers. Controlling the structure of PEDOT formation at nanoscale not only reduces the defect formation, but also facilitates tuning the morphology and direction of polymerization, thereby empowering various applications that required specifically engineered properties. For TE applicatons, chain alignment of PEDOT would enhance its mobility. However, conventional alignment methods fail since PEDOT is very difficult to dissolve in organic solvents owing to the π-π stacking of its long backbone which results in agglomeration. To overcome these difficulties, recent research has introduced the concept of using liquid crystal (LC) template to incorporate and organize EDOT molecules.

Liquid crystals are a mesomorphic phase of matter with structural and mechanical properties median between those of solid and liquid phases. They possess liquid like partial degree of freedom, while the molecules self organize into crystal like ordered structures. The LCs are mainly characterized into two types: thermotropic and lyotropic. Thermotropic LCs are formed from pure molecules and undergo phase transition with change in temperature, while lyotropic LCs are usually mixture of the material and a solvent, and their phase transition is influenced mainly by the concentration while temperature is a secondary influence. Lyotropic LCs are usually comprised of amphiphile molecules i.e. they have a hydrophilic head and a hydrophobic/ lypophylic aliphatic chain.

The shape of the self assembly of the lyotropic LC in a solvent is determined by Israelachivili model which depends on the packing parameter v_l/a_sL, where L is the length and v_l is the volume of the polymer chain, and a_s is the effective cross section area per molecule. Based on the above criteria the LC can form lamellar, hexagonal or cubic mesophases in the solvent. (Fig. 2.10)

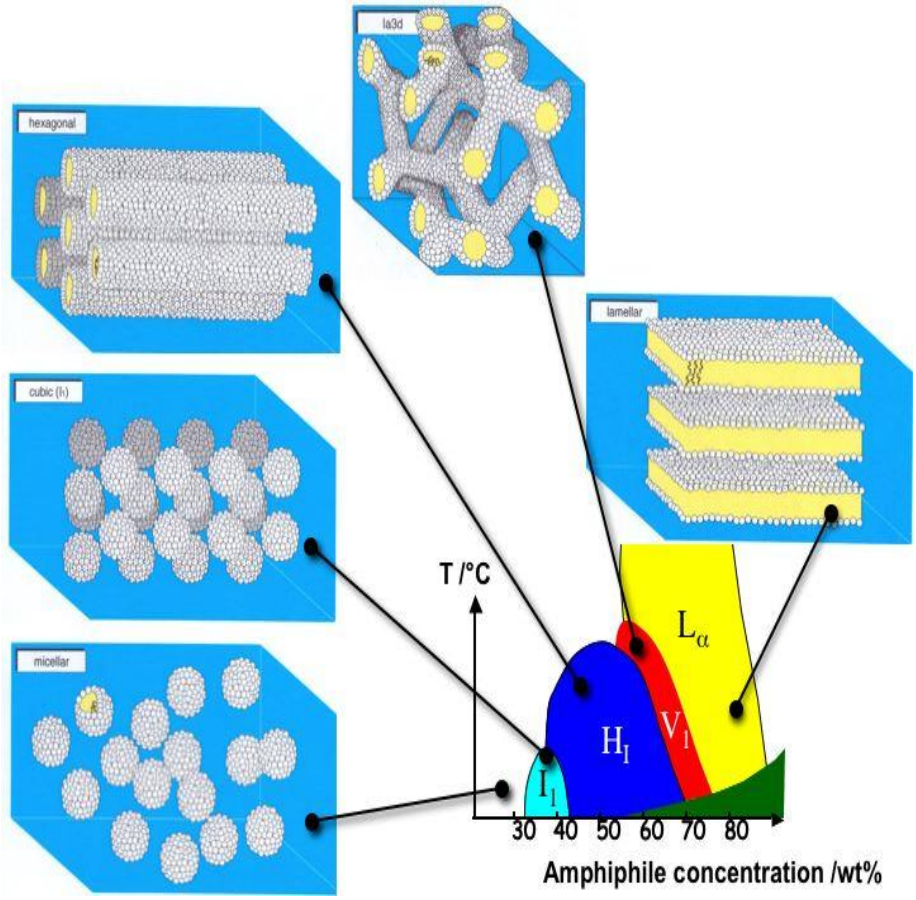

Fig. 2.10: Schematic of different phase transitions at varying amphiphile concentration and temperature.[62]

This research utilizes a lyotropic LC ($(EO)_{10}$- oleyl ether) (Fig. 2.11) which forms a hexagonal mesophase in water. This hexagonal mesophase consists of high aspect ratio hydrophobic cores which are about 3-4*nm* in diameter surrounded by an external hydrophilic shell. (Fig. 2.12) The cylindrical cores align parallel to each other and are divided by the aqueous medium. They form organized domain like structures with all cylinders in each domain oriented in a single bulk direction. They can extend up to hundreds of microns.[62]

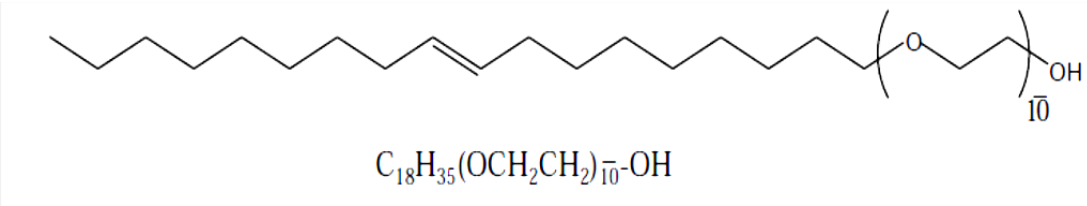

Fig. 2.11: Lyotropic amphiphile used.

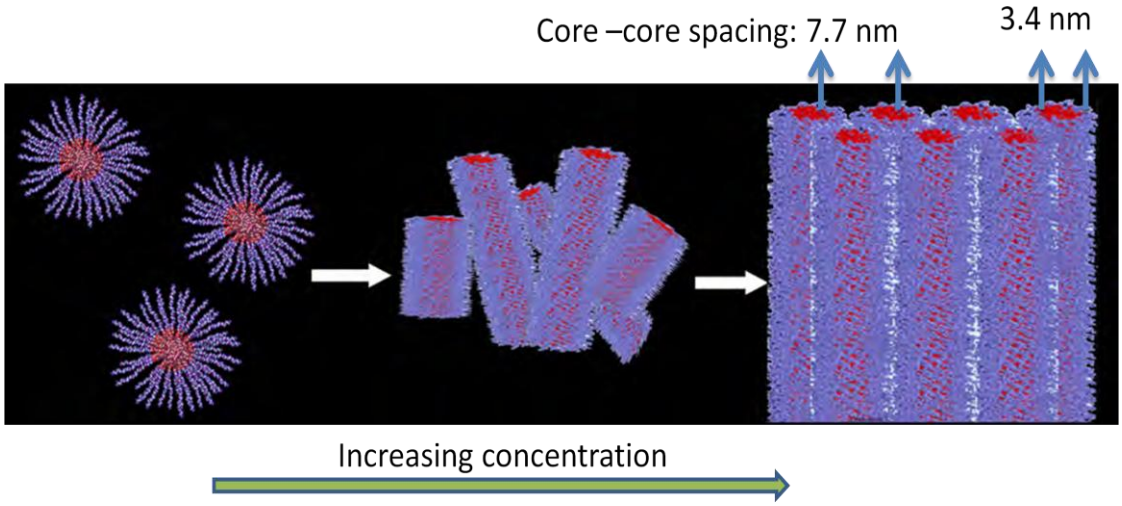

Fig. 2.12: Formation of lyotropic LC's hexagonally packed cylindrical mesophase in water at optimal concentration. Purple chains indicate the hydrophilic ends of the amphiphile and red heads indicate the hydrophobic ends.[62]

EDOT and any other hydrophobic materials when incorporated into the LC network, tend to migrate towards the core of the cylinders in the hexagonal mesophase. Thus, this network offers a relatively simple and robust technique to incorporate all the EDOT molecules into the cores of the self-organized assembly and polymerize them subsequently to obtain well controlled and aligned PEDOT chains.

2.4 Research Objective and Methodology

This research proposes the synthesis technique of organic TE thin film that can achieve the high power factor through an increase in its electrical conductivity due to increase in the charge mobility, without sacrificing the carrier concentration or the Seebeck coefficient. This is achieved by modulating the morphology of the polymer chains and incorporating high mobility material alongside the polymer chains.

The objectives involved in the synthesis were twofold: first, aligning the polymer chains relatively in a single direction and second, dispersing carbon nanotubes in a non-percolated manner in the polymer chains. Due to various advantages and promising potential, the conducting polymer selected was PEDOT.

The method chosen to achieve the first objective of aligning the polymer chains in a single net direction is to use a liquid crystalline template to mediate the molecular ordering for in situ electro-polymerization of monomers. The monomer EDOT is dispersed in a solution of a liquid crystal material along with water and then annealed according to a specific temperature profile. The non-ionic amphiphile, in the presence of water under specific temperature conditions, self assembles and forms a lyotropic liquid crystalline network in the shape of hexagonal prisms almost perpendicular to the substrate. EDOT monomers are trapped in the hydrophobic cores of the hexagonal liquid crystal structures. In-situ electro-polymerization is then carried out in the liquid crystal

matrix to polymerize the individual EDOT molecules within each core into PEDOT chains aligned perpendicular to the substrate (Fig. 2.13). The liquid crystal template is then removed leaving the aligned PEDOT domains on the substrate. The PEDOT film is then transferred onto a thin transparent insulating substrate while retaining the aligned structure.

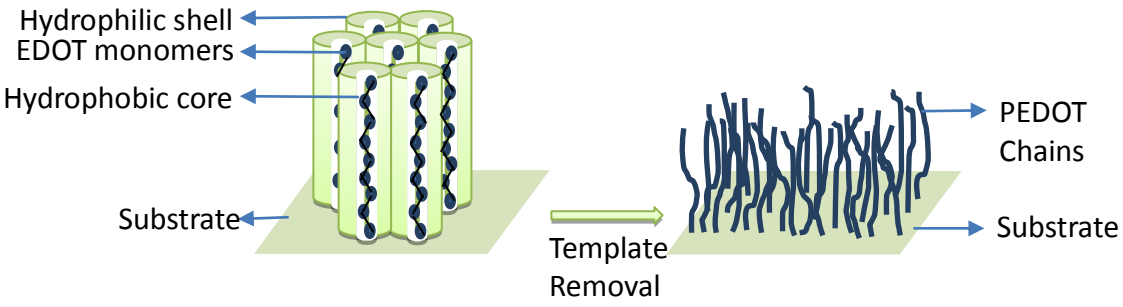

Fig. 2.13: Schematic of liquid crystal template with EDOT aligned perpendicular to the substrate subsequently polymerized aligned PEDOT and template removal.

The second objective of synthesis was to disperse non-percolated CNTs inside the polymer thin film. It can be achieved by spraying the well dispersed CNT solution onto the PEDOT film. The amount of CNTs sprayed onto the film is maintained at lower than the percolation threshold and upon spraying the solution is dried to immobilize the CNTs attached on the PEDOT chains. Also the CNTs can be incorporated within the aligned polymer chains by incorporating them initially into the liquid crystal network. (Fig. 2.14)

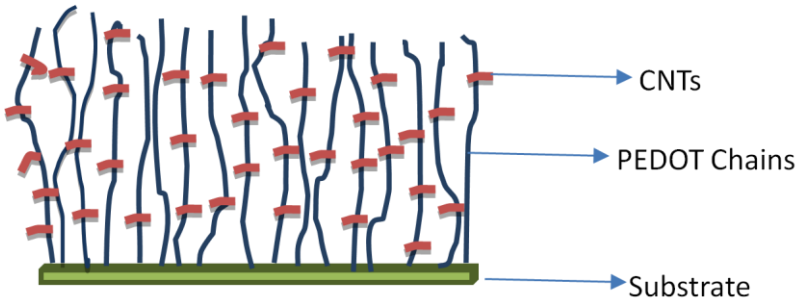

Fig. 2.14: Schematic of alignment of CNTs in a non percolated manner alongside PEDOT chains.

The oriented polymer chain structure renders better anisotropic electrical conductivity along the polymer chain backbone direction. The transverse direction to the polymer domains has a high Seebeck coefficient and relatively lower electrical conductivity due to absence of direct conductive paths and non-percolation of CNTs. Thus, taking advantage of the aligned structure and dispersing non-percolated CNTs would lead to an increase the mobility of the electrons in the individual polymer chains in transverse direction. The increase in mobility of electrons would lead to an increase in the electrical conductivity of the material in the transverse direction, without reduction of the Seebeck coefficient. Hence, the thin film can exhibit high power factor characteristics.

3 EXPERIMENTAL SET UP AND PROCEDURE

3.1 Cell Setup for LC Formation and Electrochemical Polymerization

Based on the earlier discussion on liquid crystal templating in the Section 2.3, the optimal weight ratio of 1:1 of hexagonal phase of the Poly(oxyethylene)$_n$-oleyl ((EO)$_{10}$-oleyl) to water system was used for the templating.

Several difficulties were encountered in the preparation of aligned liquid crystal template. Two varieties of cells were designed to prepare the template and polymerize EDOT.

1. First cell, as depicted in Fig. 3.1, was designed as a sandwich of an O-ring (Buna-N, McMaster) between two clear and transparent glass slides, sealed together with external pressure. This design was very important for our experiment because the transparent slides allowed us to observe and confirm the in-situ formation of the liquid crystal before proceeding to the electro-polymerization step. Since the cell was small enough to transfer and focus under the optical microscope, observations could be made directly under the polarized light without opening the cell or disturbing the template. This configuration allowed us to relate the LC domain formation to the experimental conditions and allowed us to narrow down on the best amphiphile to water ratio as well as best

annealing temperature profile. However, though this primary cell allowed us to confirm the formation of liquid crystal, it had several shortcomings:

i. The sealing of the device was not proper, and as suspected there was change in composition of the LC mixture due to evaporation of water at higher temperature. This gave rise to unevenly aligned domain structures in the LC template and also concentration of aligned domain formation on the edges of the O-ring where most water accumulated.

ii. The cell did not have any room for inserting the reference and counter electrodes for the following step of electro-polymerization.

iii. The glass slides did not function as the working electrode, making it an unsuitable configuration for electro-polymerization.

A slightly alternative configuration was also attempted by squeezing the gel directly between two glass slides separated by an adhesive film of about 75μm thickness on all edges of the slides, instead of using the O-ring.[62] But this configuration also had similar shortcomings, and the results were even worse due the entrapment of air bubbles inside the gel during the sealing process which disturbed the formation of aligned LC domains.

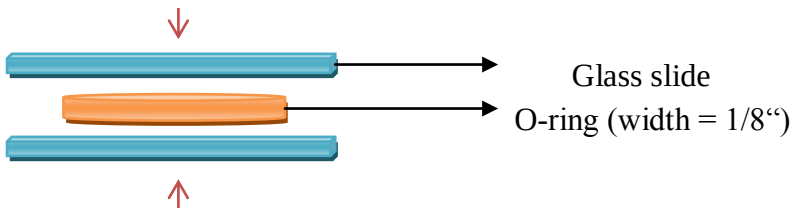

Fig. 3.1: Schematic of the glass slides and O-ring sandwich device used for confirming and observing LC domains.

2. The second cell design (Fig. 3.2) was based on the standard 3 electrode assembly for electro-polymerization. It was fabricated from PTFE cylinder as 3 parts, to eliminate the shortcomings of the first design. It was designed to hold large amount of the LC gel, rising to several mm of height to allow for insertion of all the electrodes without disturbing the lower part of the LC template that is in immediate contact with the gold plated glass working electrode. This assembly allows for complete sealing of the LC gel and prevents the formation of air bubbles or loss of water through evaporation. However, this cell also had certain shortcomings such as:

    i. Since the cell had large volume, several mm of LC gel was required to be able to insert the electrodes into the gel. This was not expensive with readily available LC amphiphiles such as $(EO)_{10}$-oleyl ether, but this would impose huge cost upon the preparation method in case of other LC materials or monomers. In that case the cell would need to be modified in lines of the first design that needed only a few mg of material.

    ii. The whole assembled cell was huge and its height did not permit in-situ observation of the LC template under optical microscope.

    iii. The large volume of the gel also meant that the annealing step needed to be modified for even slower rates of cooling because of the possibility of residual thermal stresses disrupting the aligned LC domain formation.

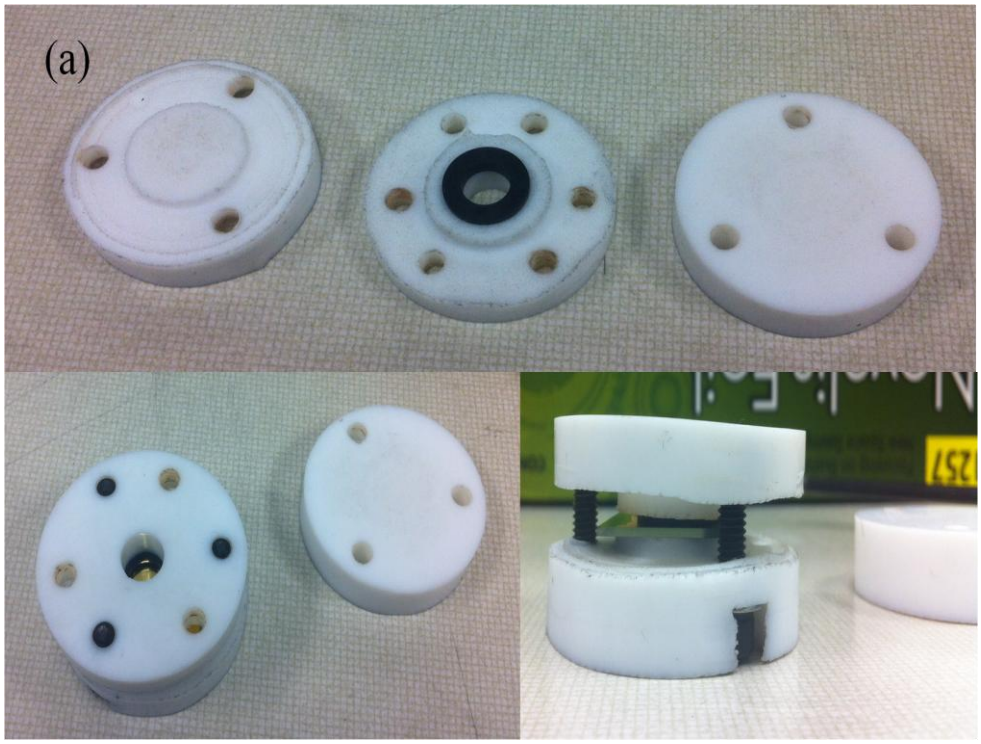

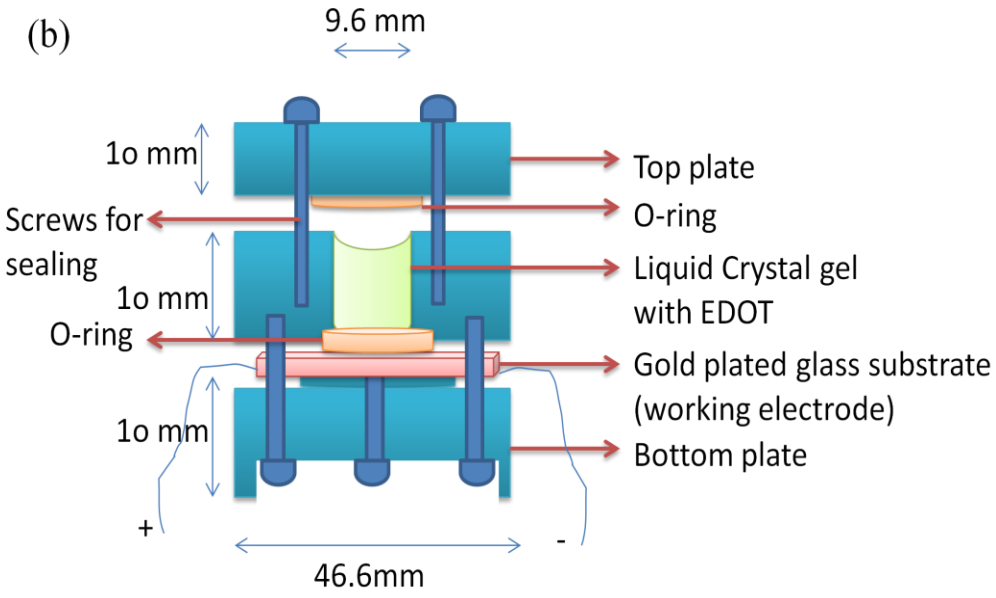

Fig 3.2 (a): Larger volume, cylindrical PTFE cell components used for LC templating; (b): Schematic of cell assembly.

3.2 Experimental Procedure for Formation of Monomer Incorporated LC Template

For the combination of $(EO)_{10}$-oleyl ether and water, the isotropization point (T_i) i.e. temperature where the LC gel flows easily due to complete disruption of order, was determined to be about $48^{\circ}C$.[62] The following steps describe the experimental procedure:

1. Poly(oxyethylene)$_n$-oleyl ether (95%, Sigma Aldrich, n~10), manufactured by ICI America under the trade name Brij-97, is produced by anionic polymerization of ethylene oxide from an oleic acid starting material. The amphiphile being 95% pure contains traces of water and remnant oleic acid. Also, due to its hygroscopic nature the amphiphile readily absorbs water from the air, and hence will generally contain 2-3% water. Thus, it was first heated at about $100^{\circ}C$ for 1 hour in vacuum (~10 *Pa)* to ensure the removal of any absorbed water vapor.[62]
2. 0.1M EDOT (99%, Bayer AG) and 0.15M tetraethylammonium perchlorate (TEAP) (95%, Acros Organics) were dissolved in 1g of pre-heated and moisture free $(EO)_{10}$-oleyl ether.[62] This mixture was ultrasonicated to evenly disperse the solutes and dissolve them partially. Perchlorates in the form of anhydrous crystals are usually explosive in nature and must be handled with care. However, TEAP was not found to be explosive and it was safe when used as described.
3. 1g of de-ionized (DI) water pre-heated to about $75^{\circ}C$ was added to the above mixture. The mixture was then vigorously mixed to dissolve all the remaining

solutes to form a clear viscous solution. The temperature of the solution was maintained about 70-75˚*C*, so that it still remained in viscous liquid form and well above the isotropization point.

4. The substrate over which the LC template was formed was chosen to be in lab prepared e-beam evaporated gold plated glass (30 *nm* Au, 100 *nm* Cr, and glass) cut into 17*mm* x 23*mm* pieces. This substrate provided an advantage as it doubled as the in-situ working electrode during the electro-polymerization process without the need for disturbing the aligned LC domains to insert an external anode. The substrate was cleaned in a standard iterative process through ultra-sonication (15 *min* each) using isopropyl alcohol, ethanol, acetone, and DI water to remove any organic and inorganic impurities, and dust particles. The substrate was then held in place in the PTFE cell and the whole assembly was pre-heated to about 70˚*C*.
5. The clear LC gel was then carefully transferred into the cell avoiding the formation of any air bubbles. The cell was then sealed completely on the top and inserted into a programmable oven to follow the preset temperature profile of controlled cooling to ensure that residual stresses do not arise, and large LC domains are obtained.

Before polymerization, it was important to heat the mixture above T_i, to about 70˚*C* and then cool down the transparent gel according to the specific annealing profile to improve the ordering of domains in the LC. It was demonstrated that cooling rates of 1˚*C/min* or

smaller result in large, well ordered LC domains that are nearly 100 μm in size.[62] The following annealing profile (Table 3.1), though not completely optimized, gave rise to the maximum domain size of over 680 μm in our case.

Table 3.1: Annealing profile of the LC cell to obtain maximum domain size.

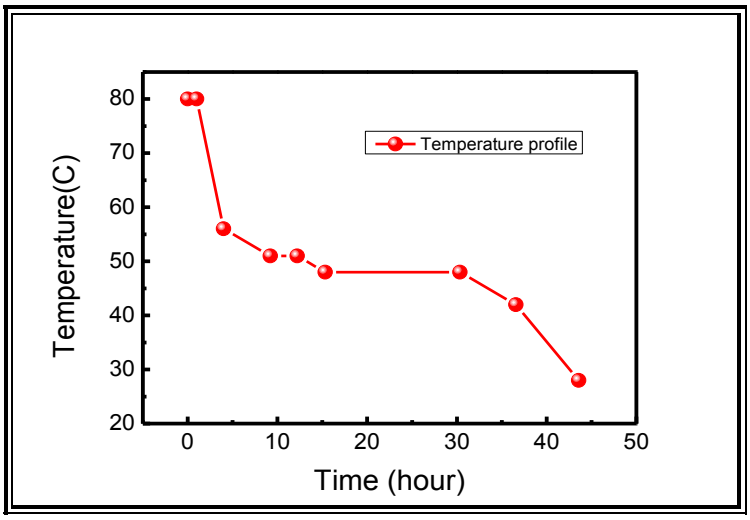

Step	**Temperature**	**Time**
1	80˚C	1 hr
2	80˚C →56 ˚C	3 hr
3	56˚C →51˚C	5hr 12min
4	51˚C	3 hr
5	51˚C →48˚C	3hr 8min
6	48˚C	15 hr
7	48˚C →42˚C	6hr 15min
8	42˚C →28˚C	7hr

The hexagonal mesophase self organizes on the gold plated glass substrate. The annealing profile starts with heating above the *Ti* to about $70^{\circ}C$, when the gel is added into the cell and sealed, followed by controlled cooling up to $51^{\circ}C$, the point at which heterogeneous nucleation is determined to begin.[62] Holding the mixture at the temperature for several hours allows for formation of a few nuclei (Fig. 3.3 (a)). Then it is cooled very slowly to 2-3$^{\circ}C$ below the *Ti* and again held there for several hours, to allow the growth of the previously formed nuclei and preventing further homogenous nucleation (Fig. 3.3 (b)). Then the gel is cooled further by $10^{\circ}C$, to complete the growth and coarsening of the LC domains. Once the temperature falls below $40^{\circ}C$, the gel's hexagonal ordered structure has essentially developed and hence it can be cooled more rapidly to the room temperature.

This procedure, though not optimized for minimum annealing time, allowed the formation of well ordered LC domains which were sized 500 – 700μm on average. This size was sufficient for our further polymerization and characterization steps. To obtain even larger domains and even better orientation, it is important to prevent any heterogeneous sites for nucleation such as surface scratches, bubbles, uneven texture on the walls, etc., which are extremely difficult. It was observed that maintaining a temperature close to *Ti* gave rise to low nucleation and high growth rates producing a coarse microstructure with large grains. On the other hand, a strong cooling with low temperature (lower than *Ti*) gave rise to high nucleation with low growth rates resulting

in fine structure with small grains. Very slow cooling rate near *Ti* is needed to avoid any thermal stress that disrupts the ordered structure.

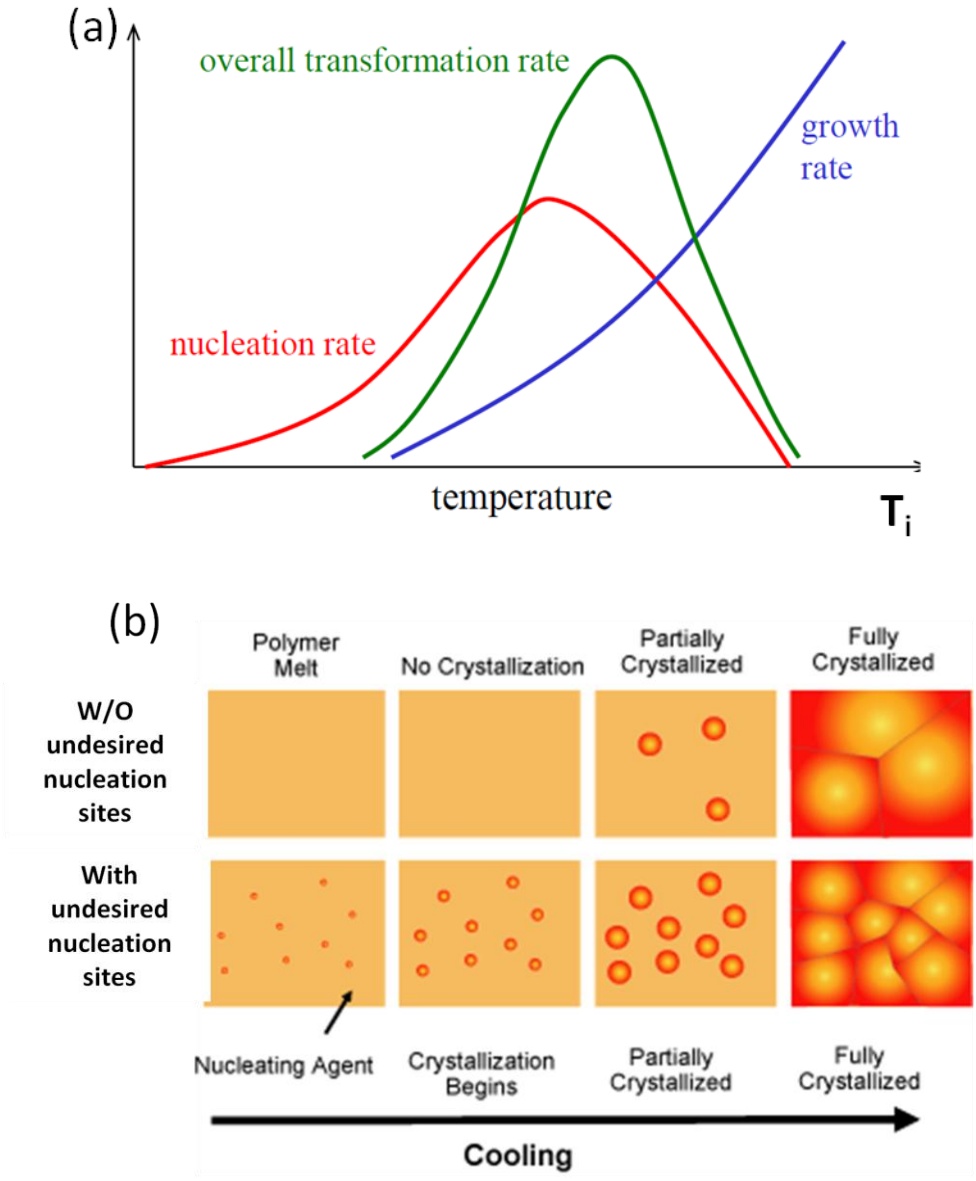

Fig. 3.3 (a): Nucleation and growth rate affecting domain size in LC; (b): Undesired heterogeneous nucleation.

3.3 Electrochemical Polymerization

There are different ways of electro-polymerizing the EDOT embedded in the aligned cores of LC gel: using constant voltage (potentiostatic), using constant current (galvanostatic), or using cyclic conditions. It was determined to be difficult to use galvanostatic conditions, owing to the unpredictable potential that might lead to over-oxidation.[62] Hence cyclic voltammetry (CV) method was chosen. It was reported that the $(EO)_{10}$-oleyl gel was stable up to an applied potential of 2.2*V*, after which it starts decomposing due to electrolysis of water at the cathode. The oxidative polymerization of EDOT monomers starts at the anode/ or the working electrode (i.e. gold plated glass substrate) when the potential goes beyond 0.9*V* vs. the reference sliver (Ag) electrode. The maximum polymerization was found to occur at the voltage of 1.3*V*, which gave rise to the highest peak in the CV diagram and also resulted in high mean current density. This was quite similar to the behavior observed during polymerization of EDOT in organic solutions.[63] Going beyond 1.4*V* leads to over oxidation and non conductive PEDOT films which is not desirable.

Fig. 3.4(a) shows the cell setup used for electro-polymerization and Fig. 3.4(b) shows the formation of PEDOT after several cycles indicated by the change in color from transparent to dark bluish-green film on the substrate. Cyclic Voltammetry was performed using an E&G Princeton Applied Research potentiostat model 236A. Fig.

3.4(c) shows the CV curve during electro-polymerization of PEDOT in the $(EO)_{10}$-oleyl template, performed by sweeping the potential repeatedly for 20 cycles from 0 – 1.3*V* (anodically vs. Ag) at scan rate of 50 *mV/s* (with a negative cathodic current).

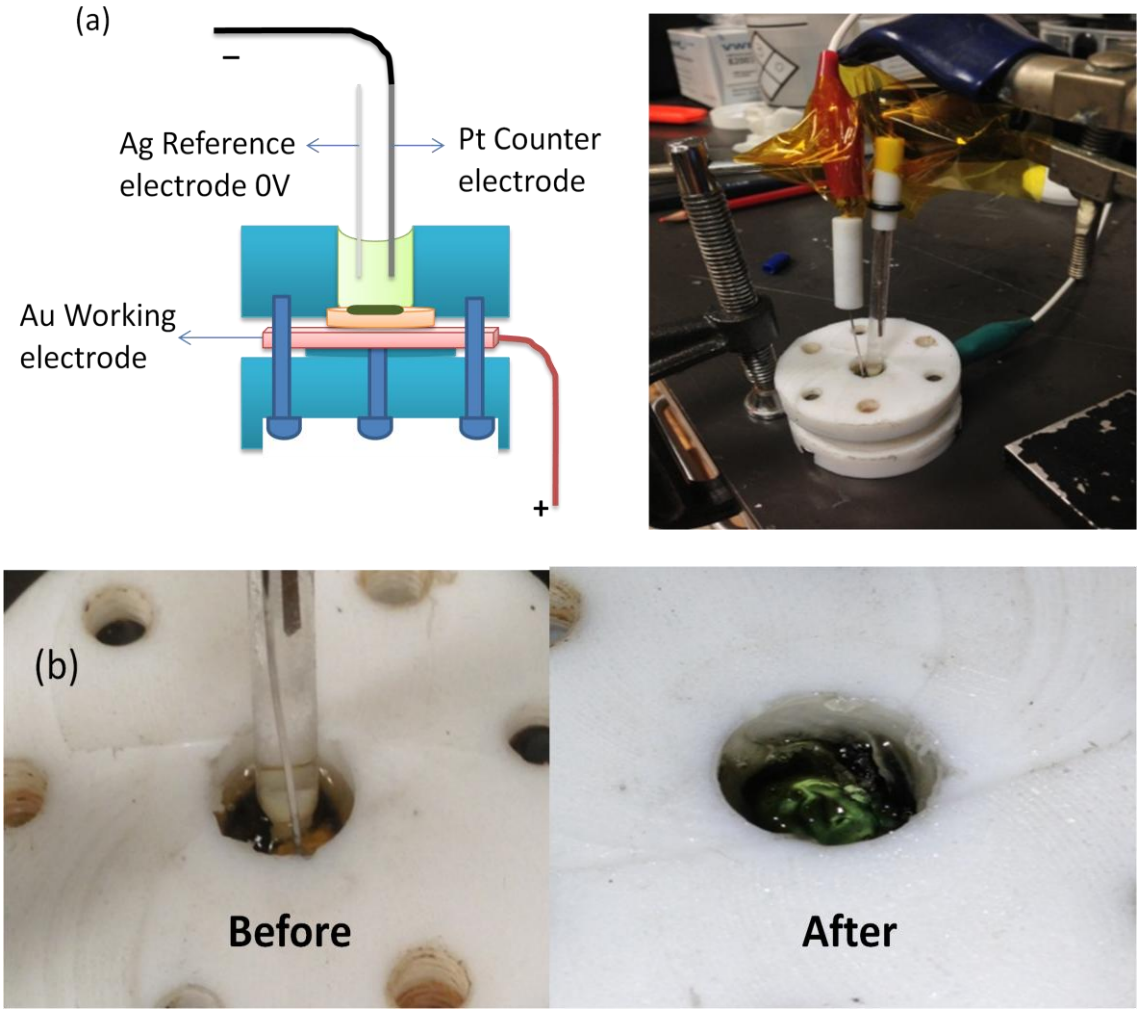

Fig. 3.4 (a): Cell set up for electro-polymerization; (b): Polymerization indicated through electro-chromic transformation from transparent to dark green after PEDOT formation on the gold substrate; (c): I-V curves of the cyclic voltammetry during polymerization.

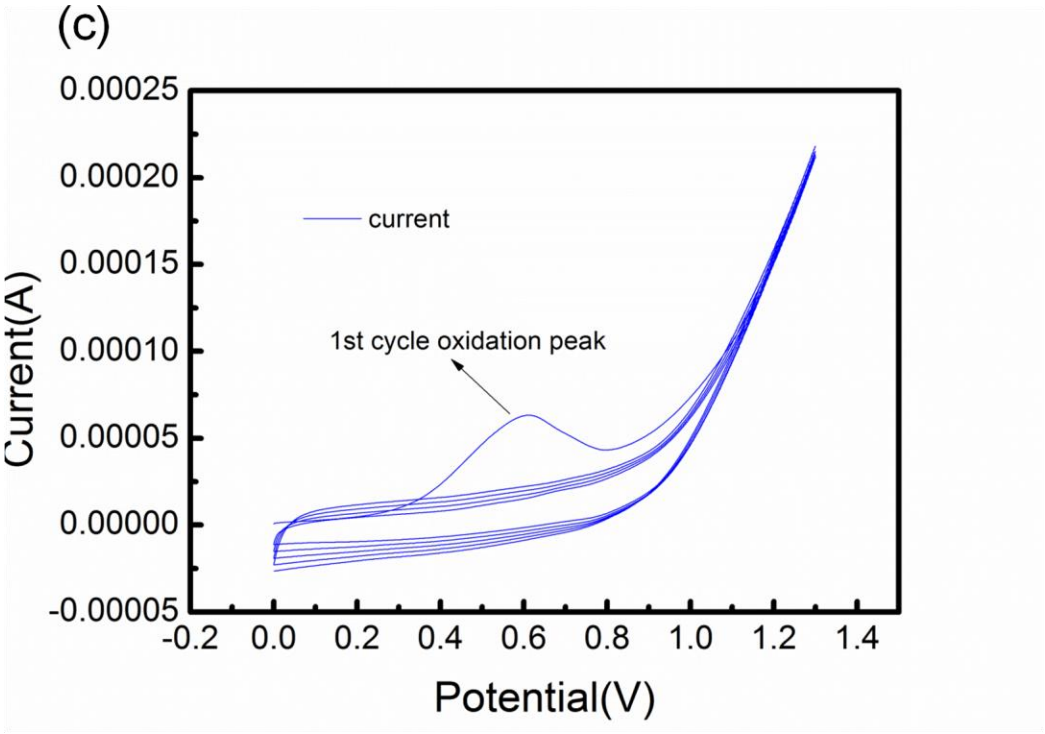

Fig. 3.4 (continued)

Fig. 3.4(c) shows the electro-polymerization curves obtained during the cyclic voltammetry process for polymerizing EDOT in several cycles. The input for the cyclic voltammetry experiment consists of a linearly ramped potential in the working electrode and then further after reaching a set potential, the working electrode's potential ramp is inverted. The curves show the current plotted against the voltage. It can be observed from the curve that there is a significant amount of hysteresis observed between the oxidation and reduction curves for each cycle. This is an indicator that the polymerization is still occurring after the first cycle as these curves indicate a non-reversible electrochemical activity occurring inside the sample. Had the polymerization

been completely achieved in the first cycle, the remaining cycles would not have produced hysteresis in the I-V curves. Also, there is a negative current observed when the reduction reaction takes places. This is an indicator of reversal of potential at the working electrode, which now releases back the electrons it has taken from the electrolyte during the polymerization process earlier. Also, the oxidation peak has a different shape as compared to the reduction curve, which is an indicator of an irreversible electro-polymerization occurring inside the solution and this corresponds to the formation of aligned PEDOT polymer chains inside the LC template.

It was observed that only the first cycle produced a remarkable peak in the CV curve showing a broad oxidation peak, centered at $0.6V$ which indicated the polymerization of EDOT. However, no peaks could be observed for further cycles. Excess EDOT molecules do gradually add on the surface and thicken the PEDOT film throughout the process. It was observed that with higher cycling currents (i.e. higher scan rate), the core part of the cylindrical gel was polymerized, while with lower cycling currents, the peripheral part was polymerized. Also, using smaller currents produced polymerized PEDOT which is more uniform and contained well in ordered domains.

3.4 Removal of Template and Thin Film Transfer

After electro-polymerization, the LC template was washed away by immersing the whole gold substrate containing the PEDOT film and the LC template into a solution of

acetone, ethanol and DI water mixed in the equal ratios. It was left in this solution for about 2 hours at which point most of the LC template is dissolved. The substrate is then washed with DI water and dried in air. During the later investigation of electrical conductivity of the electro-polymerized PEDOT film, contrary to the expectations, lower values were observed. The cause of low conductivity was investigated to be associated with residue of LC template still remaining on the PEDOT film even after washing. (Refer to Section 4.2.2) Therefore, the washing procedure was later modified to immerse in the above solution for overnight instead of 2 hours with replacement of the solution every 2 hours for the first 6 hours. This helped in further removal of the LC template, although not completely, as was demonstrated by slight improvement of the electrical conductivity values. Dichloromethane was also used as a solvent to remove the remnants of LC template.

The transfer of the film from the conducting gold (Au) substrate onto an insulating substrate was quite essential for cutting the film into thin strips and measuring the electrical conductivity values. Several different substrates were experimented with as described below:

1. Poly-acrylic acid (PAA): The PAA solution was drop casted onto the gold plated glass substrate containing PEDOT film and heated at about $70^{\circ}C$ for 1 hour (Fig. 3.5). After complete drying, it was found that the PEDOT film on Au could be almost completely detached by carefully lifting off the polymer (Fig. 3.6). The PEDOT was also observed to have retained its ordered structure when observed

under the polarized optical microscope (POM). However, the polymer film was rigid and developed cracks on cutting the PEDOT film into thin strips.

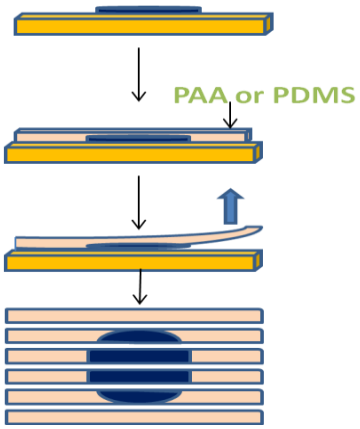

Fig. 3.5: Transfer of aligned PEDOT film.

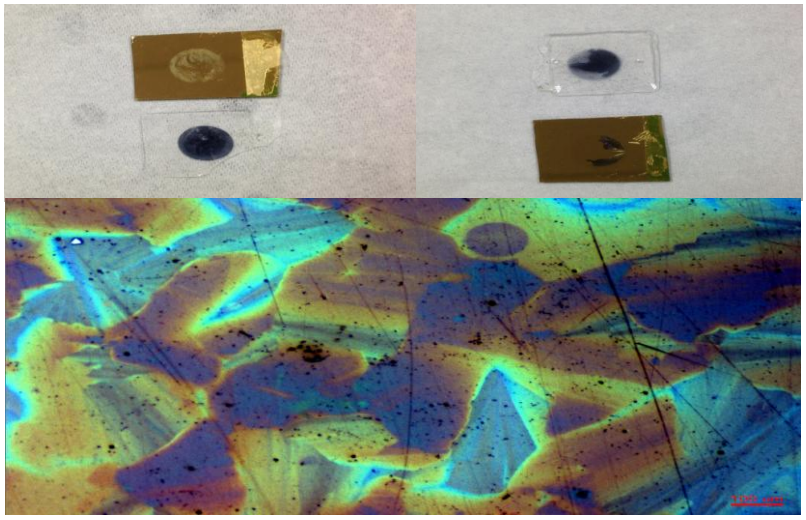

Fig. 3.6: Transfer of aligned PEDOT film on PAA substrate.

2. Sylgard 184 Elastomer or Polydimethylsiloxane(PDMS): This insulating polymer came as the separate elastomer base and a curing agent which had to be mixed

together in the ratio 10:1 respectively just before drop casting the mixture onto the *Au* substrate containing PEDOT film. The solution layer was then cured at 80˚*C* for 2 *hrs* to complete the formation of cross bonds within the polymer substrate. This substrate was flexible, but it could only lift the PEDOT film partially off the gold plated glass substrate (Fig. 3.7). The partially lifted film retained the ordered structure when observed under POM.

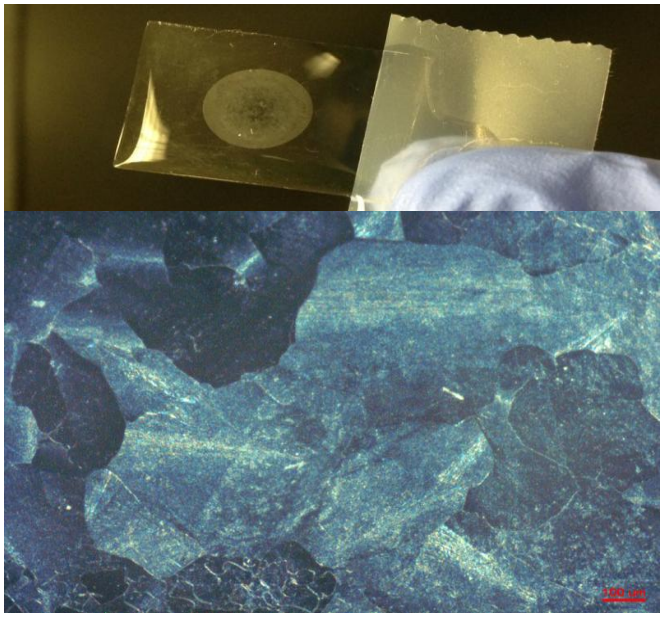

Fig. 3.7: Transfer of aligned PEDOT film on PDMS substrate.

3. PAA and PDMS combined substrate: To mitigate the disadvantages in both the above polymer films, a combined substrate containing layers of both PAA and PDMS was utilized where the individual polymer characteristics complemented

each other to facilitate the lifting and cutting process. The following steps outline the transfer process (Fig. 3.8):

i. PAA solution is spin coated as a thin layer on Au/PEDOT substrate using SCS 6800 spin coater, where the parameters for spin coating were: ramp = 5*s*, dwell = 10*s*, speed = 1500*rpm*.

ii. The sample was then heated at 50˚*C* in vacuum (~10 *Pa*) for 1hour for drying.

iii. PDMS was then drop casted on PAA film with mixture of elastomer base: curing agent as 10:1 respectively.

iv. The sample was again cured at 50˚*C* for 1 hour.

v. The cured PAA/PDMS film was carefully lifted from the substrate using a razor blade.

The PEDOT film was found to be attached to the transparent, insulating and partially flexible polymer film. Since PAA was in contact with the PEDOT film, most of the PEDOT could be lifted off and PDMS being on the farther side, ensured partial flexibility of the film. The film could now be cut with razor blade into thin strips for further characterization and property measurement.

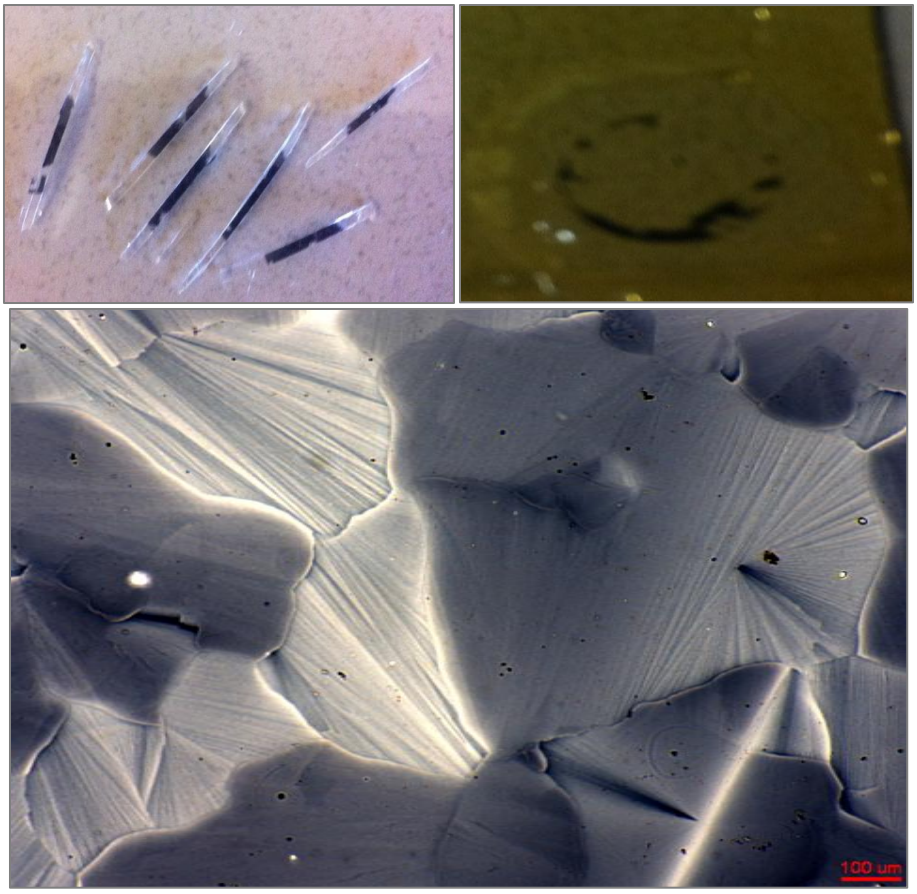

Fig. 3.8: Transfer of aligned PEDOT film on PAA and PDMS combined substrate.

3.5 Doping of the Film

Three different p-type dopants were selected for incorporating in different concentrations to study the effect of doping on the electrical conductivity of the aligned PEDOT. These were Camphorsulfonic acid (CSA), Iron (III) Chloride ($FeCl_3$) and Dimethylsulphoxide (DMSO). The dopants were incorporated in two different ways:

1. After formation of aligned PEDOT:

Different concentrations of the dopants were dissolved in ethanol and dropped onto the PAA/PDMS polymer substrate containing aligned/ unaligned PEDOT. This was allowed to dry partially for about 30 minutes after which the PDMS layer could be lifted off physically and the PAA layer could be subsequently dissolved by immersing the PEDOT film in DI water. This process allows for doping the surface of the bare aligned PEDOT film and depositing the film directly onto a micro device/ platform for further characterization studies.

2. Before the alignment of LC and electro-polymerization of PEDOT:

   The influence of incorporating the dopant within the aligned structure of PEDOT without disrupting the alignment was also studied. To achieve this, different concentrations of the dopants were dissolved into hot poly (oxy-ethylene) oleyl ether even before the addition of DI water during the formation of the LC gel. This allowed for the even dispersion and incorporation of the dopant along with EDOT molecules into the LC template.

3.6 Incorporation of CNTs into Aligned PEDOT Thin Film

CNTs are highly hydrophobic in nature and tend to agglomerate in water. Hence it is very important to disperse them well using some surfactants to prevent the formation of CNT bundles. A solution of well dispersed CNTs was prepared using the standard procedure as described below:

1. 2*mg* of P2 CNT (Carbon Solutions Inc.) was mixed with 8*mg* of SDBS (Sigma Aldrich) and 20*g* of DI water in a closed vial.
2. The vial was sonicated sequentially using by bath type sonicator (Branson) for 1 hour and pen type sonicator (MISONIX) for 2 hours.
3. Step 2 was repeated for 2 more times (3 times in total)
4. The solution was centrifuged (Centrifuge - Fisher Scientific) in small vials at 12000 *rpm* for 20 *min*. The clear supernatant was carefully collected after centrifuge and placed in a closed vial.
5. Step 2 was then repeated again for 1 more time.

Similar to doping, CNT incorporation could also be achieved in two different ways:

1. After formation of aligned PEDOT:

   The PEDOT film was transferred on to the polymer substrate and heated to a temperature of about 200˚*C* and the CNT solution was sprayed using a spray gun, for different amounts of time like 5*s*, 15*s*, 25*s*, etc to obtain different concentrations of CNT on the PEDOT sample (Fig. 3.9) and hence the percolation threshold was determined. The spraying was conducted in iterative intervals involving 5*s* of spraying and 5*s* of drying, to ensure CNT is well dispersed and dried directly on the PEDOT surface. Since the sample was heated, the CNT solution air sprayed dried completely upon contact with the film surface. This process allowed for CNT incorporation on the PEDOT surface rather than the bulk sample.

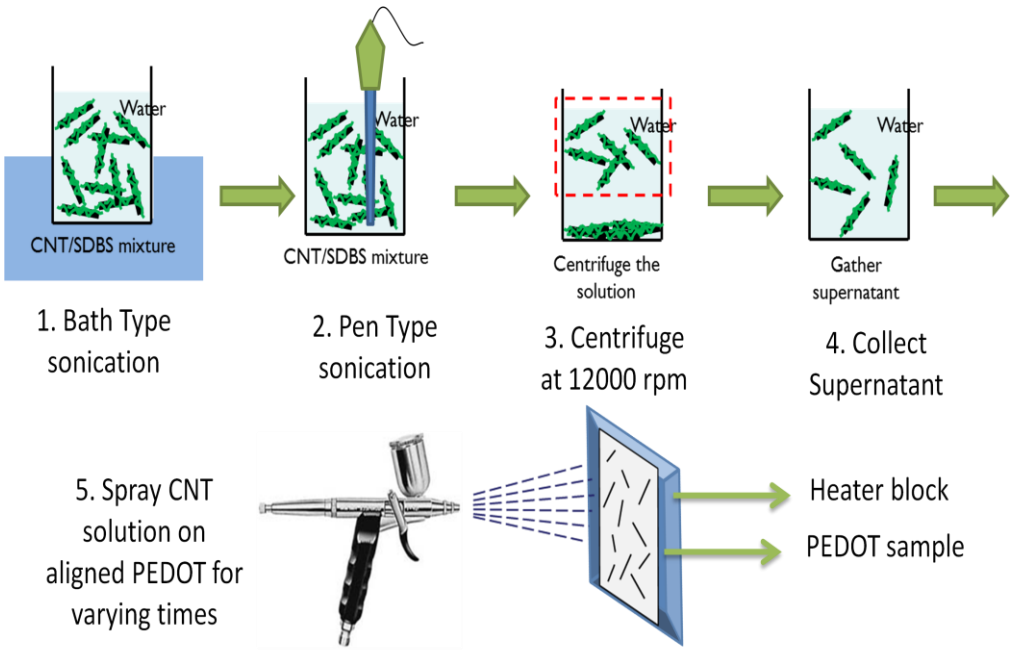

Fig. 3.9: Process of CNT dispersion and spraying on the PEDOT samples.

2. Before the alignment of LC and electro-polymerization of PEDOT:

   To incorporate CNTs uniformly within the LC template along with the EDOT molecules even before alignment and electro-polymerization step, the $1g$ of DI water used for LC formation was replaced with $1g$ of dispersed solution of CNT in DI water. This mixture was then allowed to from LC template and subsequently electro-polymerized in the same exact manner as before to obtain bulk CNT incorporated aligned PEDOT thin film.

4. CHARACTERIZATION AND ANALYSIS

4.1 Characterizing Alignment of PEDOT

After electro-polymerization, the LC template was washed away as described in the previous sections and the substrate was dried thoroughly. The PEDOT thin film which adhered to the substrate was then transferred onto a transparent PAA/PDMS substrate as described in the previous section. This thin film was observed under the polarized optical microscope (POM) (Olympus) for characterizing the alignment of the PEDOT chains. The polarized optical microscope consisted of two extra lenses, the polarizer and the analyzer, for polarizing the light in the desired orientation. The analyzer lens could be rotated such that its orientation could be parallel, at an angle or perpendicular to the orientation of the polarizer lens. Fig. 4.1 (a) shows the POM set up under bright field with the polarizer lens, analyzer lens and PEDOT sample in place. When the polarizer and analyzer are oriented perpendicular to each other, and there is no sample placed in between them, then no light will be reflected from the analyzer lens as it would be completely absorbed because of the mutually perpendicular orientations. This is called the cross-polarized orientation and only crystalline structures or those which materials exhibit a certain order when placed in between the two lenses would be able to render a preferred orientation to the polarized light and reflect off some light. Any amorphous material without any preferred orientation would not reflect off any light and hence appear completely black under the cross-polarized POM. Fig. 4.1 (b) shows the rotation

and cross-polarized orientation of the polarizer and analyzer lens. Liquid crystals, when placed under crossed-polarizers demonstrate birefringence pattern i.e. periodic dark and bright regions, due to the ordered structural domains.

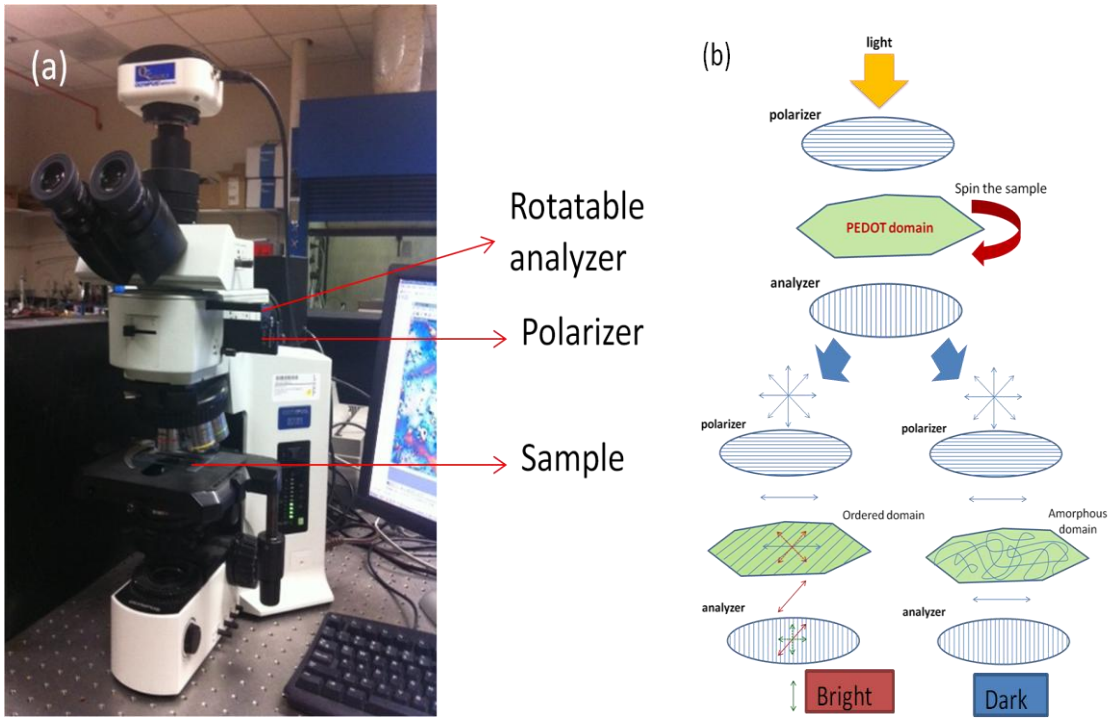

Fig. 4.1 (a): Optical microscope set-up with polarizer and analyzer lenses (POM); (b): Schematic of birefringence pattern exhibited by an ordered assembly in LC compared to an amorphous material observed under crossed polarizers

When observed under POM, the microstructure of the PEDOT film confirmed the templating effect hypothesis of the LC gel. The electro-polymerization of the PEDOT without any LC templating (i.e. by replacing the $1g$ of $(EO)_{10}$-oleyl ether in the preparation process with $1g$ of DI water) resulted in a uniform and featureless thin film under the optical microscope and a completely dark image under POM. But the PEDOT

thin film grown from the $(EO)_{10}$-oleyl LC gel showed aligned polymer domain formation that was complementary to the domain formation observed in LC. Fig. 4.2 shows a few optical microscope images of the LC templated PEDOT with aligned domains. The largest domain size obtained was 680µm. Varying colored domains represent varying refractive indices due to non-uniform thickness.

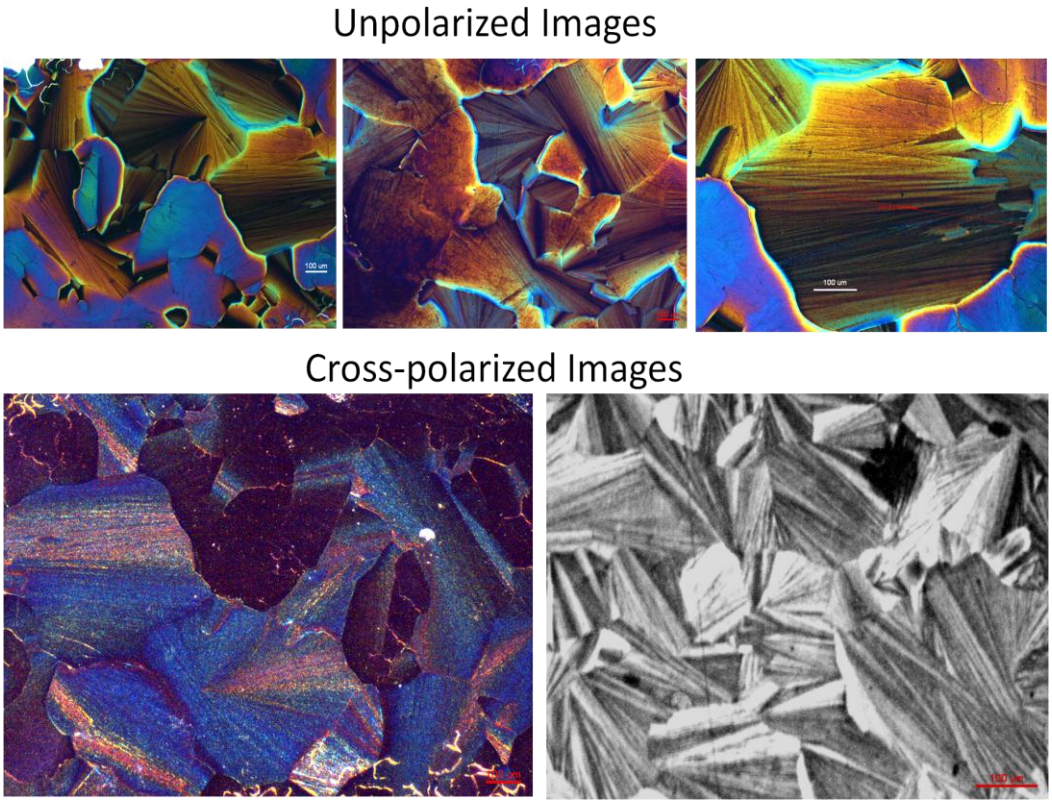

Fig. 4.2: Unpolarized images showing domain formation in aligned PEDOT thin film and POM images showing bright and dark domains under cross polarized light; scale bar on all images indicates 100µm.

POM could be used to determine the orientation of each individual aligned PEDOT domain. This could be achieved through observing the brightness changes during

rotation of a single PEDOT domain between the cross-polarized POM. The aligned domains that always remain dark upon rotation between cross-polarized light could be inferred to be oriented parallel to the incident light i.e. perpendicular to the substrate surface. This is because the polymer chains in these domains do not alter the incoming polarized light's orientation and hence do not contribute a preferred orientation to the polarized light. This unaltered polarized light when passed through the perpendicularly oriented analyzer, is completely absorbed leaving behind a completely dark image of that domain.

On the other hand, the LC domains that switch between dark and bright upon rotating 45˚ correspond to aligned domains with the director orientation at some non-perpendicular angle to the substrate surface. They could either be completely parallel to the substrate in which case they appear as the brightest spots upon rotation, or at some angle between parallel and perpendicular orientations. These domains exhibit an alternating bright and dark appearance upon rotation because their aligned polymer chains could reflect off the polarized light that strikes them and change its orientation through an angle to render a preferred orientation which depends on their director angle. Thus the reflected altered polarized light now has two components, one parallel to the cross-polarized analyzer and another perpendicular to it. The perpendicular component is completely absorbed by the analyzer, but the parallel component is allowed to pass through the analyzer thereby rendering some brightness to the domain. Fig. 4.3 shows

the schematic of orientation of cross-polarized light when reflected off an aligned sample under rotation through 45˚.

The process of domain orientation indicates that the anisotropic LC environment strongly influenced the polymerization of PEDOT. The PEDOT domains when observed under the optical microscope also reflected off various colors indicating that each domain had a different refractive index. This could be due to the variant thickness of each domain. During the electro-polymerization process, the EDOT monomer had to diffuse to the Au electrode surface to get oxidized into polymer chain. But this diffusion occurs more easily through the hydrophobic cores when they offer least resistance to the diffusion path. Therefore, from the varying thickness, it can be co-related that the polymer might have grown fastest in cores aligned normal to the substrate or in other words, parallel to the electric field. A parallel or angled alignment of the cores requires EDOT molecules to either cross through aqueous/hydrophilic region of the LC or to diffuse at an angle to the external electric field in order to reach the substrate. Thus the least growth might have occurred in hydrophobic cores that were oriented along the Au substrate.

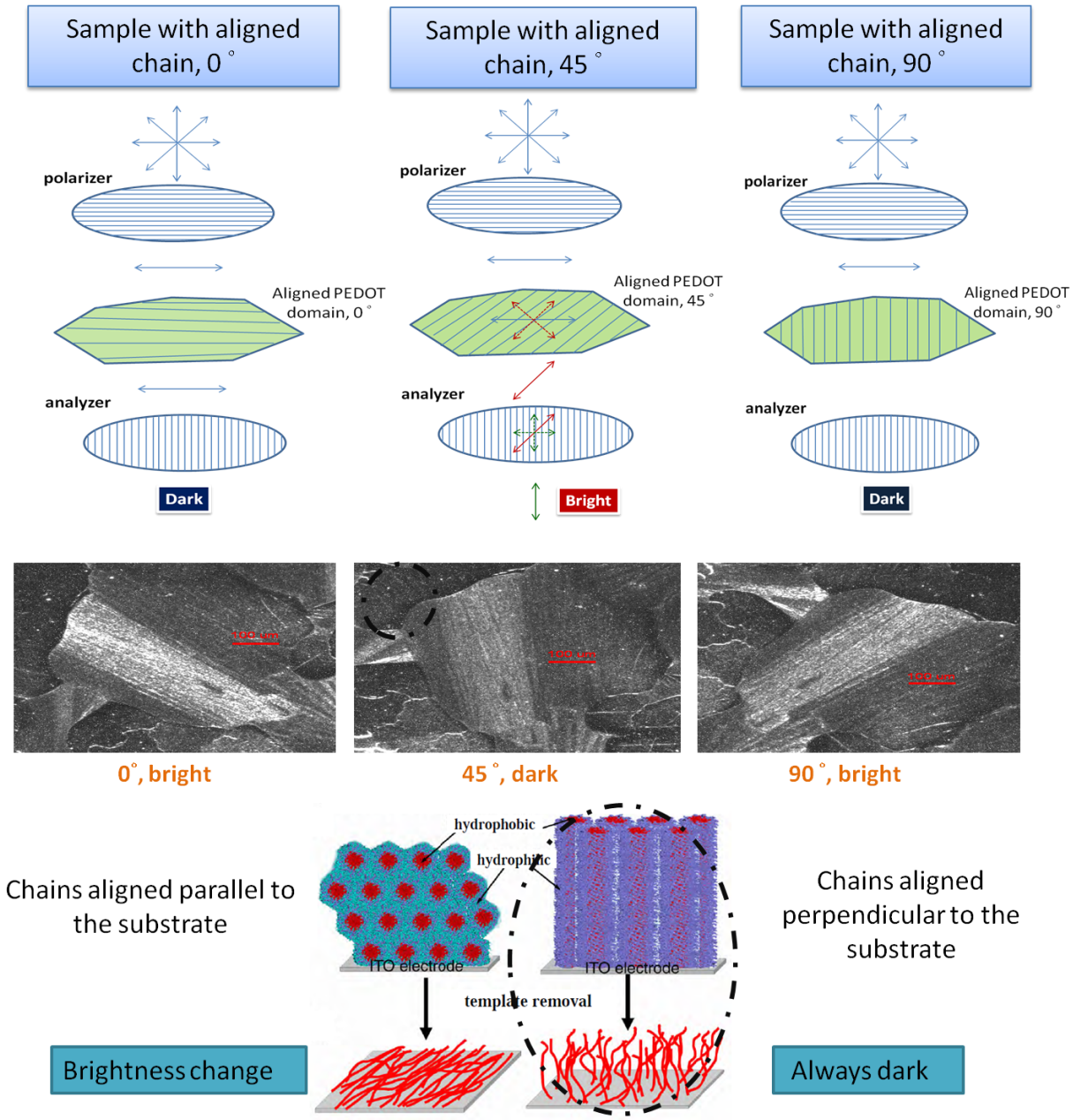

Fig. 4.3: Schematic of rotating a single aligned PEDOT domain under cross polarized light to observe the alignment of the director of the polymer chains; Rotation through 45° shows brightness change for domains oriented non-perpendicular to the substrate while domains perpendicular to the substrate always remain dark.

The LC itself exhibited a birefringence pattern and the polymer thin film exhibited almost a similar copy of the birefringent domains as the LC from which it was polymerized. Even upon soaking these polymer films in solvents like CH2Cl2 for several hours to completely remove the traces of LC template, these films were observed to be stable and the birefringence pattern was not affected. A control sample in which PEDOT was electro-polymerized from EDOT and TEAP in DI water (without the addition of $(EO)_{10}$-oleyl) mixture at room temperature. This control PEDOT film showed uniform and amorphous structure and did not exhibit any domain texture or birefringence under POM. (Fig. 4.4) This indicates that the PEDOT film produced itself has no liquid crystalline like structure, but the polymerizations of the monomers in the hydrophobic cores that are oriented at different angles generate the anisotropy and domain structure. This anisotropy induced by LC template is locked into the PEDOT structure due to its highly insoluble and hydrophobic nature.

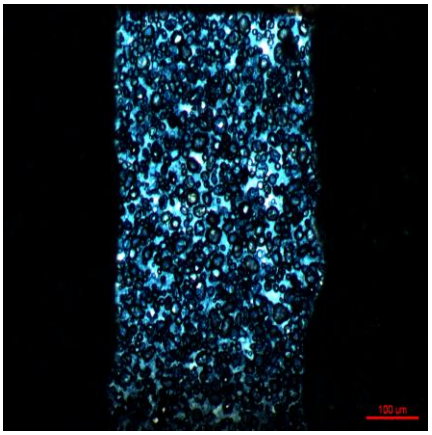

Fig. 4.4: Optical microscope image of electro-polymerized amorphous PEDOT thin film (prepared without LC templating) showing absence of alignment and domain formation.

4.2 Electrical Conductivity Characterization

PEDOT films can have drastically varying σ values depending on the method of preparation. σ values between the range of 10 to 10,000 Sm^{-1} have been reported in the literature and the influencing factors include the level of doping, introducing counter-ions and incorporating different additives during the film preparation.[64-68] After preparation of the aligned and electro-polymerized PEDOT thin films as described in Section 3, these films were transferred onto an insulating substrate to study the electrical conductivity values.

4.2.1 Bulk electrical conductivity

The aligned PEDOT thin film strip, after transferring to an insulating substrate of PAA/PDMS, was tested for electrical conductivity using the 2 probe method, with a probe station. (Fig. 4.5) The local resistance of the film was measured by passing current through the two probes and simultaneously measuring the voltage developed. The resistance values in the order of tens of MΩ were obtained for thin films with thickness approximately in the range of 200*nm* and a diameter of about 0.8*cm*. This resulted in the bulk electrical conductivity values in the order of 10^{-2} *S/m*. But since the bulk PEDOT film was composed of several individual domains which had different orientations, the bulk value indicated an isotropic measurement and not the anisotropic improvement in the electrical conductivity due to alignment of polymer chains in one direction. Fig. 4.6 represents the multi-domains with different orientations present between the two probe

tips placed 2 *mm* apart. Therefore, in order to measure the anisotropic influence of polymer chain alignment on the electrical conductivity value, measurement of σ of each individual aligned domain must be obtained.

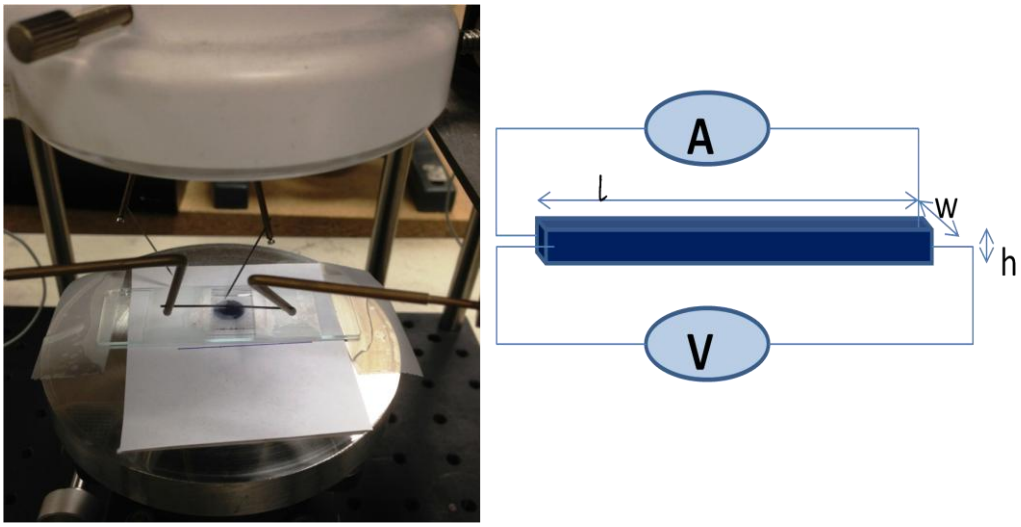

Fig. 4.5: Probe Station with 4 probes and PEDOT sample on an insulating substrate; alongside schematic for 2-wire resistance measurement.

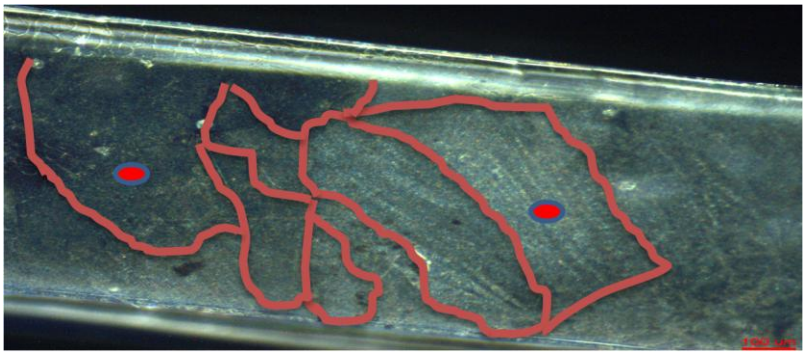

Fig. 4.6: Multiple domains with different alignments between the two probes placed about 2*mm* apart.

4.2.2 Single domain electrical conductivity measurement

In order to test the anisotropic electrical conductivity of the aligned PEDOT sample, the micro-device shown in Fig. 4.7 was used. This device consisted of 4 parallel gold lines at a separation distance of approximately 95μm. The PEDOT strip could be laid across these conductive lines and the resistance value of the domain containing the two inner probes could be measured. The four parallel lines also allow for the 4-wire resistance measurement, in which current could be passed through the two outer probes and voltage could be recorded along the two inner probes. This method is better than the 2 probe method as it eliminates the contribution of any contact resistance between the sample and the probe tips. For a domain of dimensions approximately 25.75μm in length, 13.64μm wide across the two inner probes and with thickness approximately 0.184μm, the resistance was about 43.2$M\Omega \pm 5M\Omega$ which translates to σ value of about 0.066 Sm^{-1}. This value is about three orders of magnitude lower than the literature value.[55]

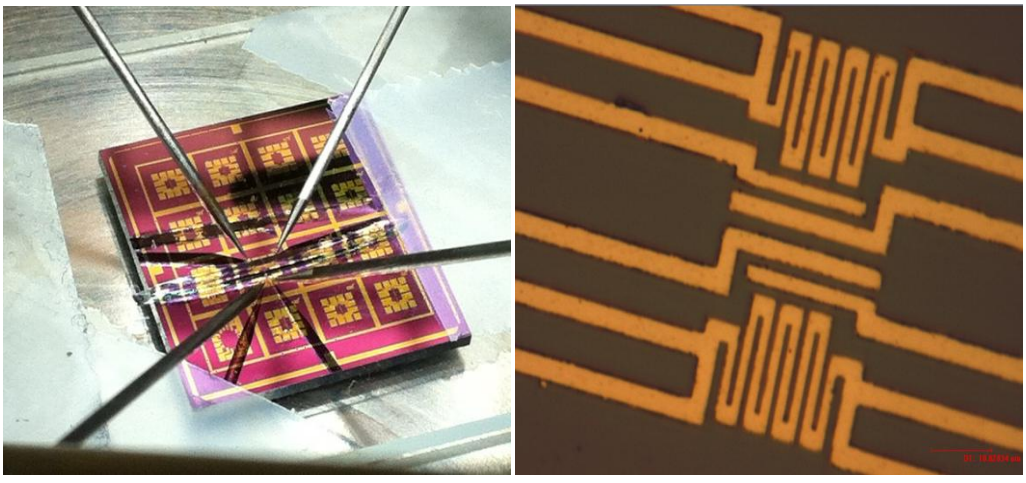

Fig. 4.7: Microdevice containing 4 parallel gold lines; scale bar indicates 10μm.

There might be several factors that could have adversely affected the σ value. Some of them include:

1. Micro –crack formation: During the removal of the PAA/PDMS substrate from the PEDOT sample, some micro-cracks were observed to be formed due to stress exerted during PDMS layer lift off. (Fig. 4.8) These were prevented in later experiments by using a thinner spin coat of PAA and reducing the temperature of baking the drop casted PDMS layer.

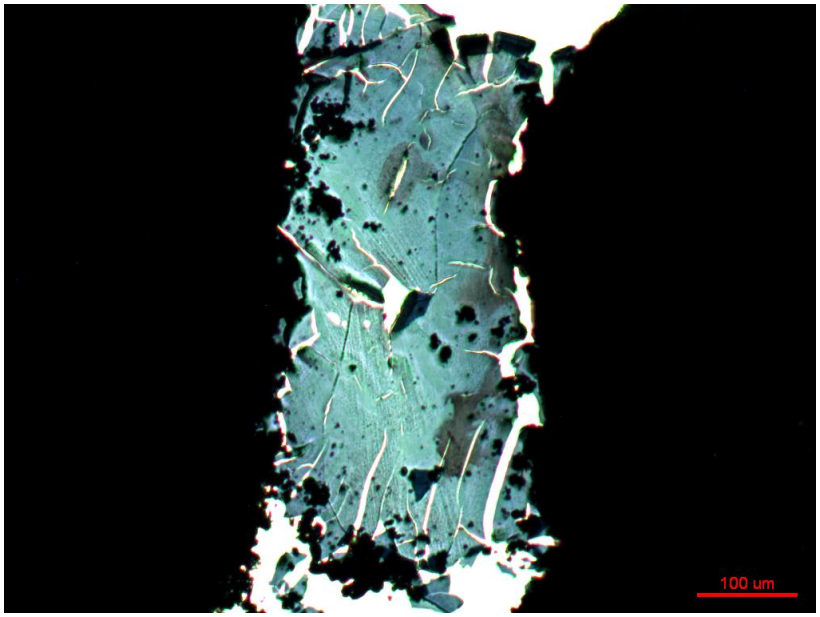

Fig. 4.8: Micro-crack formation within the PEDOT thin film during PAA/PDMS substrate removal; scale bar indicates 100μm.

2. Contact resistance due to air gaps: Since the PEDOT thin film is attached to the Au plated micro-device physically with the help of surface tension during ethanol evaporation; there might not be strong contact between the film and the gold

surface. Hence the air gaps and poor contact could have been a factor for the high resistance. To avoid this problem, a different substrate for the σ measurement has been used. Silver paint was spread over a masked tape of about 400μm in width, as a thin layer over a glass slide. After the paint partially dried, the tape was peeled off to expose the bare glass slide surface of about 400μm with conductive Ag paint electrodes on either side. (Fig. 4.9) The PEDOT thin film was then transferred directly onto this configuration while the paint was still partially wet, thereby ensuring a good contact of the PEDOT domains with the conductive electrodes. With this configuration, σ values improved approximately three times over those on the gold micro-device.

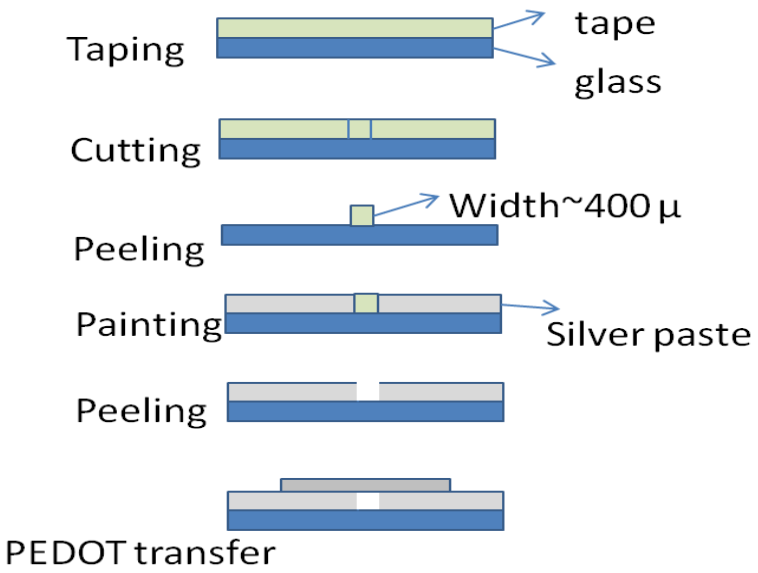

Fig. 4.9: Schematic of preparation of the silver paste electrodes on glass substrate using a masking tape.

3. Residual of LC template: There could still be some remnants of the LC material within the aligned and polymerized PEDOT thin film. Since the LC material itself non-conductive, it could form barrier between the PEDOT polymer chains and contribute to high electrical resistance. Hence, to confirm this, non templated electro-polymerized PEDOT, which was prepared by replacing the $(EO)_{10}$-oleyl amphiphile with equal amount of DI water instead, was studied. This non-aligned electro-polymerized PEDOT does not exhibit any domain structure and shows no birefringence pattern under the optical microscope.(Fig. 4.4) This sample exhibited σ value of about 55.2 Sm^{-1}, which is about two orders improvement over the aligned sample and almost comparable to the literature value of electrical conductivity. This proves that the low conductivity in the aligned sample might have been caused by the remnants of the LC template. Hence, to overcome this, solvents such as dichloromethane have been used for longer overnight immersion times. This resulted in further thorough removal of the LC template, as can be demonstrated by the change in refractive index of the PEDOT domains as exhibited in Fig 4.10. The σ values could be improved by about one order of magnitude.

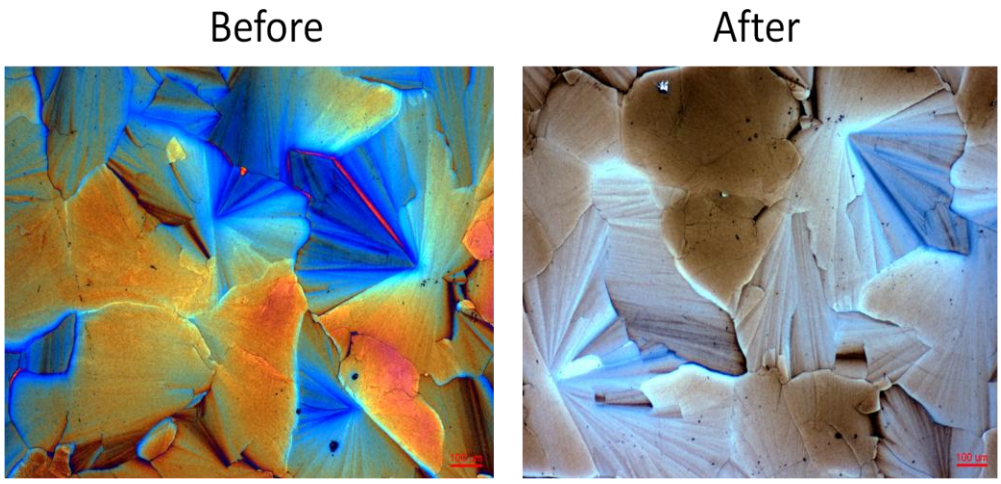

Fig. 4.10: Change of color and therefore refractive index of the PEDOT thin film after washing for longer time with CH_2Cl_2 as the solvent.

4. On the other hand, for a non-rectifying junction or the Ohmic contact, the resistance measured is the true resistance of the PEDOT sample. Thus, to test the type of contact, 4-wire resistance measurement technique was used to observe the *I-V* curves. The type of junction could be deferred from the shape of the *I-V* curve. The aligned PEDOT sample with some dispersed CNTs sprayed on the sample and placed on the micro-device was tested for *I-V* curves with an in-lab made testing station. (Fig. 4.11 (a), (b)) The curve obtained was straight line passing through the origin, which demonstrates that the contact was an Ohmic contact. (Table 4.1)

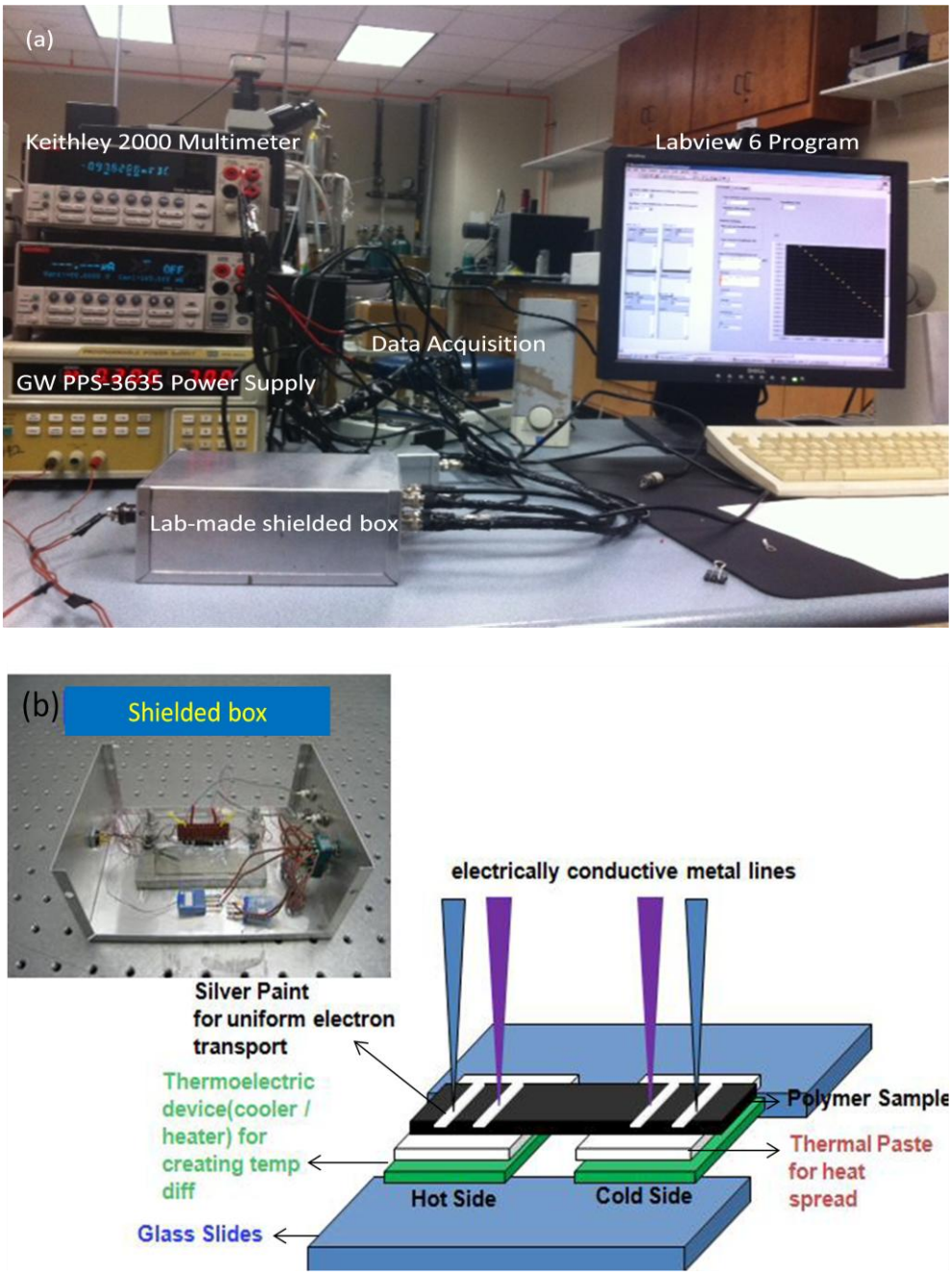

Fig. 4.11 (a): Experimental station set-up for measuring σ using 4-wire resistance method to eliminate the influence of contact resistance; (b): Inner view of in-lab made shielded box for measurements.[69]

Table 4.1: Straight line I-V curve obtained for electro-polymerized PEDOT thin film with 4-wire resistance method.

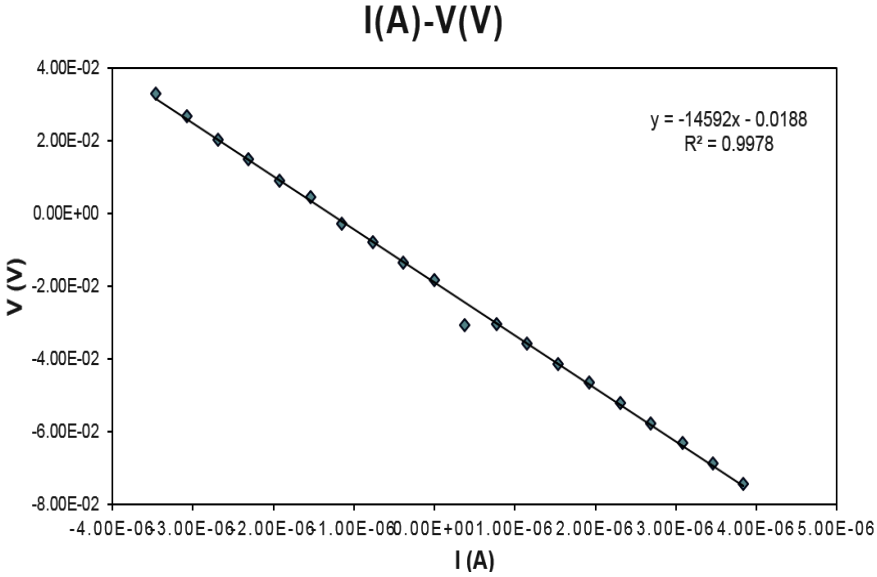

4.2.3 Effect of doping on electrical conductivity

Adding dopants through the two processes described in Section 3.5 improved the σ value. When the dopants were drop casted onto the polymerized and aligned PEDOT, nearly one order improvement in electrical conductivity could be observed. For PEDOT domain over the silver paste electrode assembly, with dimensions L = 13.64μm, W = 25.75μm, t ~ 0.18μm, with DMSO drop casting on the PEDOT surface, σ increased from 0.06812 *S/m* to 0.1794 *S/m*. For a different PEDOT domain, with CSA as the dopant, σ increased from 0.31 *S/m* to 8.917 *S/m* and for $FeCl_3$, σ increased to 1.8985 *S/m*. Thus CSA showed the best doping effect on σ of PEDOT thin film. Table 4.2 shows the effect of increase in σ after doping CSA externally on the PEDOT surface.

Table 4.2: Increase in σ values (S/cm) by approximately 10 fold after doping in 4 different PEDOT thin film samples.

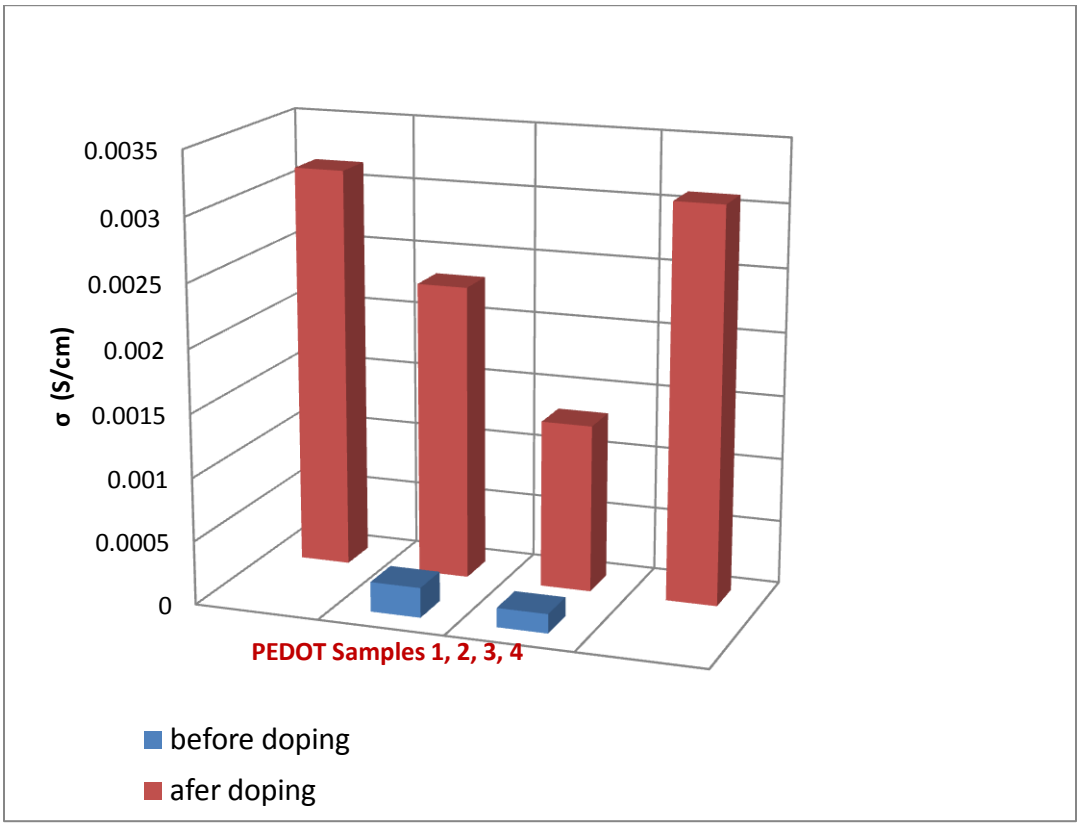

As described in Section 3.5, dopants could also be incorporated in different concentrations internally within the bulk of aligned PEDOT domains by altering the initial LC formation recipe. For the recipe that was prepared by incorporating 0.1*M* CSA (23*mg*) into the LC gel mixture of 0.1*M* EDOT, 0.15*M* TEAP dissolved in poly(oxyethylene)$_n$-oleyl ether, σ value increased by about two orders of magnitude. Fig. 4.12 shows the optical microscope image of 0.1*M* and 0.2*M* CSA dispersed within the aligned PEDOT domains. The optimal dopant incorporation (0.1*M*) did not disturb the formation of the aligned structure in the LC template, but excess dopant incorporation

(0.2*M*) did not produce any ordering within PEDOT structure and resulted in a poorly polymerized thin film.

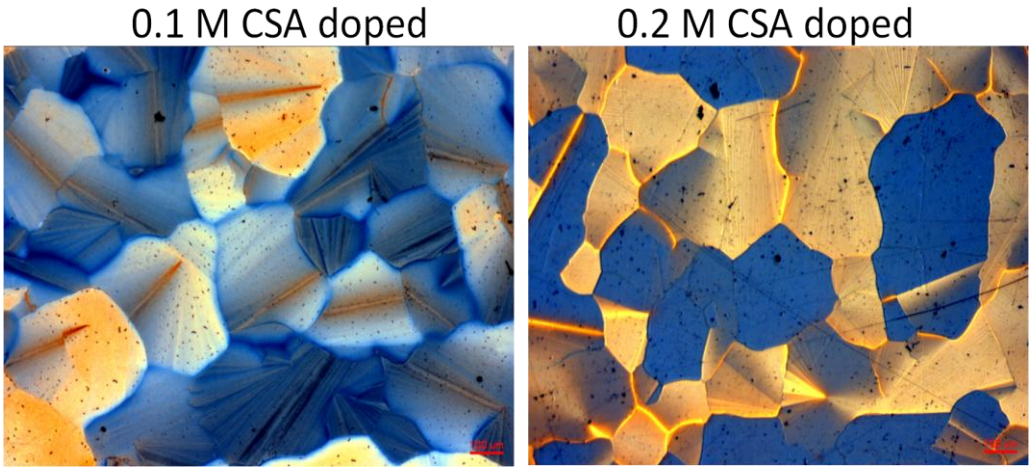

Fig. 4.12: Optical microscope images of dopant dispersion within aligned PEDOT domains in 0.1*M* and 0.2*M* CSA doped PEDOT thin films.

4.2.4 Effect of CNT incorporation on electrical conductivity

As described in Section 3.6, CNT could be incorporated in two ways: externally or internally. For CNT incorporation on the PEDOT thin film by spraying on the PEDOT surface, it was first necessary to determine the percolation limit, to prevent formation of any connective network/ paths in a transverse direction to the aligned polymer chains. Formation of such percolated networks is unfavorable for improvement of the power factor of the TE material as they would contribute to increase in k. Hence, to determine the percolation limit, CNT solution was prepared and sprayed for different times on a bare glass substrate and the resistance values were measured to determine the optimal spray time when percolation limit is reached. (Fig. 4.13) Fig. 4.14 shows the SEM

images of the CNT sprayed samples on a bare glass substrate. It could be observed that the network of CNTs starts forming only for spray times higher than 45*s*.

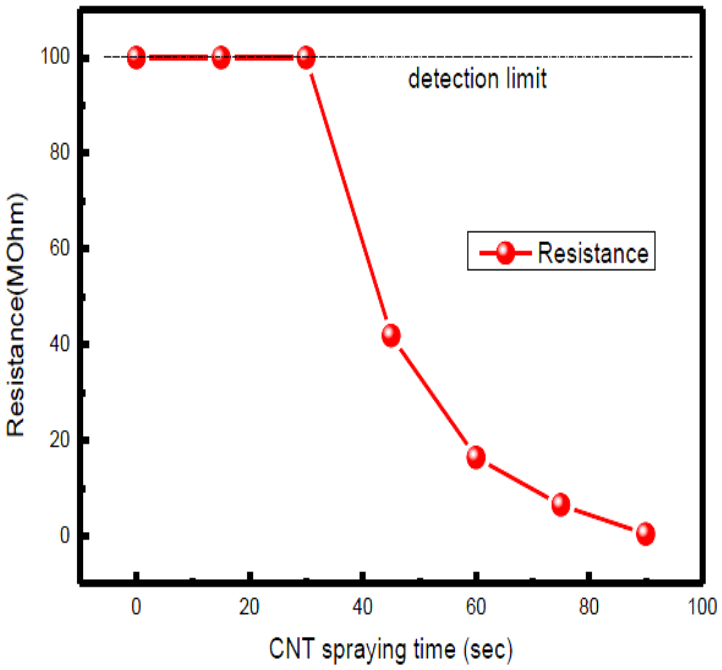

Fig. 4.13: Resistance values ($M\Omega$) for different spray time(s) of CNT solution to detect the percolation limit of CNT spraying on bare glass substrate. Sharp fall in the resistance curve indicates the percolation threshold.

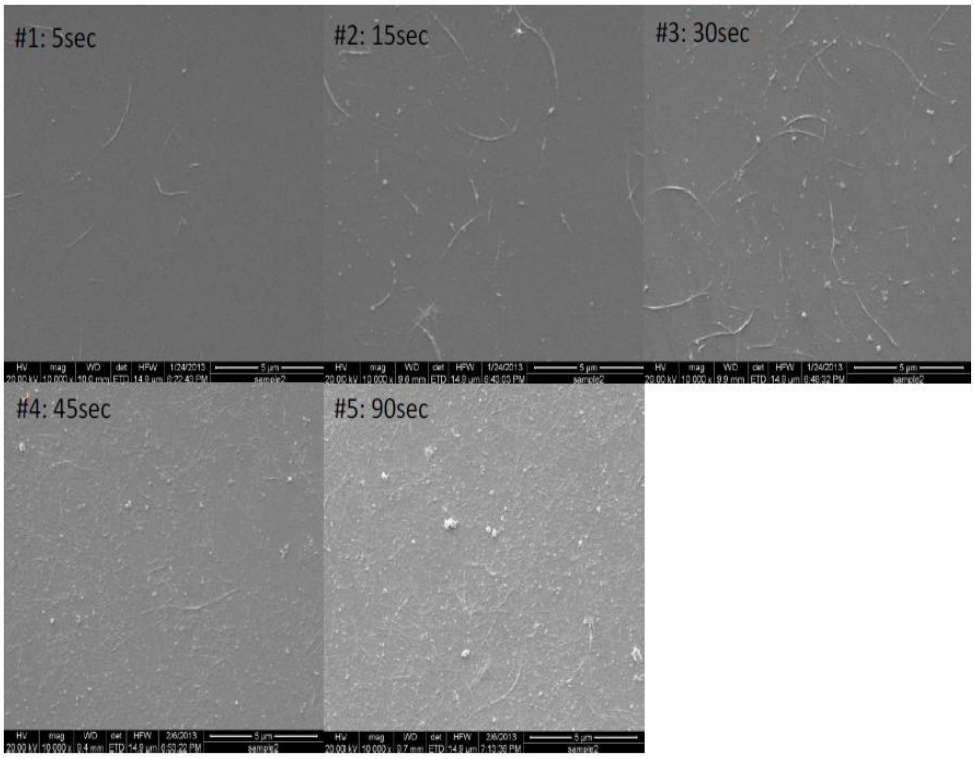

Fig. 4.14: SEM images of CNT sprayed on to bare glass substrate for different spray times.

The resistance values after spraying CNT solution on PEDOT samples were measured, but no conclusion could be reached about the trend of σ with different spray times. That was because the PEDOT samples needed to be heated to very high temperatures of about $200^{\circ}C$ during the process of CNT spraying. At such temperatures, PEDOT film degraded gradually and σ decreased and thus even if CNTs contributed to increase in σ, it was over shadowed and the trend showed an overall decrease. Since the two effects could not be decoupled, no firm conclusion could be drawn.

On the other hand, internally incorporating CNTs within the aligned domains of PEDOT resulted in improvement of σ by about two orders of magnitude as compared to plain aligned PEDOT thin films. Fig. 4.15 shows the optical microscope image of the CNT bundles dispersed within the aligned PEDOT domains. It could be observed that even though CNT was well dispersed through sonication, it still tended to form bundles within LC template, but that did not disturb the formation of LC template.

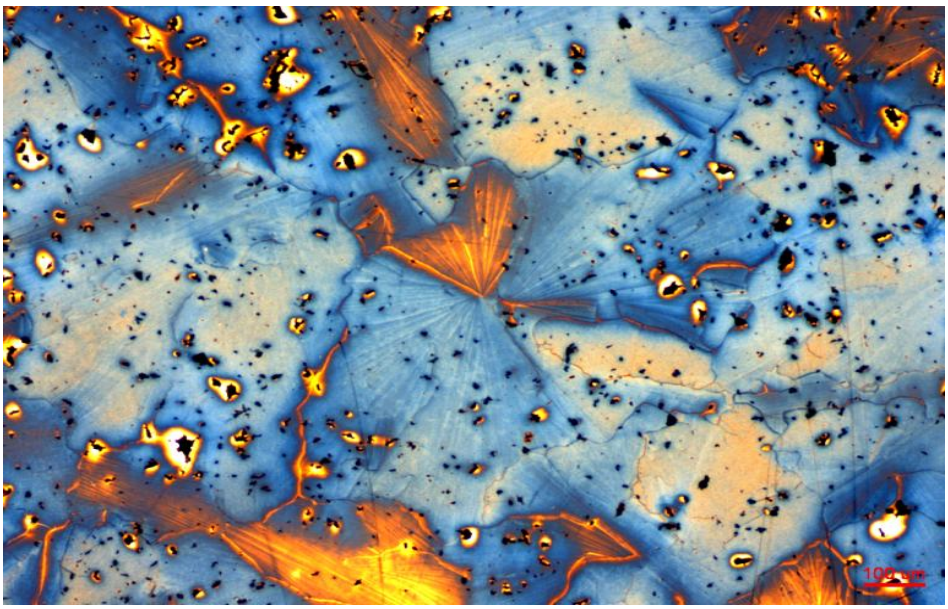

Fig. 4.15: Optical microscope image of CNT incorporation and dispersion into bulk of aligned domains in PEDOT thin film; Scale bar indicates 100μm.

5. SUMMARY AND CONCLUSION

Aligned PEDOT thin films were prepared through the facile route of electro-polymerizing monomers EDOT in lyotropic, hexagonally self-organized LC template. These conducting polymer thin films were robustly transferred onto insulating substrates as well as measuring micro-devices for characterization. CNTs and various dopants were incorporated and dispersed into the bulk of aligned PEDOT thin films through dissolution into the LC gel before electro-polymerization. They were also incorporated externally onto the surface of the PEDOT thin films through spraying and drop casting respectively. The thin films were characterized for bulk orientation within individual domains through polarized optical microscopy and the electrical conductivity within each domain was measured using 2-probe and 4-wire resistance methods. This research demonstrates that the electrical conductivity of the aligned polymer thin film could be controlled through two orders of magnitude through incorporation of dopants and CNTs. This increase was achieved through controlling the mobility of the charge carriers within the polymer chains through influencing the morphology of the polymer (alignment of polymer chains) and incorporation of non-percolated CNTs and dopants over the individual polymer chains. This provided a facile route for increasing the electrical conductivity of PEDOT without affecting the number of charge carriers, and thus without negatively affecting the thermal conductivity or Seebeck coefficient.

This research is only a small introduction to a novel concept for engineering a high power factor organic TE material through controlling mobility to increase electrical conductivity and thus not sacrificing Seebeck coefficient. Further investigation of this concept could involve optimizing CNT concentration in the LC template to achieve the best power factor for aligned PEDOT, orienting CNT in the transverse direction to the polymer chains using A/C electric field, rendering the PEDOT film as free standing, measuring the orientation of PEDOT chains through WAXS techniques and characterizing σ based on domain orientation, experiment with smectic phase LC templates to form PEDOT thin films, etc. There is a great potential for future work to convert this promising concept into practically viable device and exploit the advantages offered by flexible, light weight, low cost and easily processable organic thermoelectric materials for empowering the bendable electronics industry.

REFERENCES

1. Weik, M. H. The ENIAC Story. *http://ftp.arl.mil/mike/comphist/eniac-story.html* (accessed March 13th, 2014).

2. Ball, P. *Nature* **2012**, *7428*, 174-176.

3. Nordqvist, C. *MNT* **2010**, *1390*.

4. Xia, Y.; Rogers, J. A.; Paul, K. E.; Whitesides, G. M. *Chem. Rev.* **1999**, *7*, 1823-1848.

5. Someya, T. *IEEE Spectrum* **2013**, March 13th, 2014.

6. Kohlstädt, M.; Grein, M.; Reinecke, P.; Kroyer, T.; Zimmermann, B.; Würfel, U. *Solar Energy Mater. Solar Cells* **2013**, *0*, 98-102.

7. Bubnova, O.; Crispin, X. *Energy Environ. Sci.* **2012**, *11*, 9345-9362.

8. Riffat, S. B.; Ma, X. *Appl. Therm. Eng.* **2003**, *8*, 913-935.

9. Chen, H.; Goswami, D. Y.; Stefanakos, E. K. *Renewable and Sustainable Energy Reviews* **2010**, *9*, 3059-3067.

10. Heremans, J. P.; Jovovic, V.; Toberer, E. S.; Saramat, A.; Kurosaki, K.; Charoenphakdee, A.; Yamanaka, S.; Snyder, G. J. *Science* **2008**, *5888*, 554-557.

11. Jinushi, T.; Okahara, M.; Ishijima, Z.; Shikata, H.; Kambe, M. *Mater. Sci. Forum* **2007**, 1521-1524.

12. Ioffe, A. F. *Semiconductor Thermoelements and Thermoelectric Cooling;* Infosearch Ltd: London, 1957.

13. Rowe, D. M.; Min, G. *J. Power Sources* **1998**, *2*, 193-198.

14. Stevens, J. W. *Energy Conversion and Management* **2001**, *6*, 709-720.

15. Rowe, D. M. *Renewable Energy* **1999**, *1–4*, 1251-1256.

16. Yodovard, P.; Khedari, J.; Hirunlabh, J. *Energy Sources* **2001**, *3*, 213-224.

17. Smith, K. *NREL/TP* **2009**, *540-44247*.

18. Peltier, J. C. *Ann. Chem.* **1834**, *LVI*, 371-387.

19. Howard, R. E.; Lidiard, A. B. *Discuss. Faraday Soc.* **1957**, 113.

20. DeVilbiss, R. Thermoelectric thermal regulation systems. *http://www.electronics-cooling.com/1996/05/thermoelectric-thermal-regulation-systems/* (accessed February 23rd, 2014).

21. Yim, W. M.; Rosi, F. D. *Solid-State Electronics* **1972**, *10*, 1121-1140.

22. Venkatasubramanian, R.; Siivola, E.; Colpitts, T.; O'Quinn, B. *Nature* **2001**, *6856*, 597-602.

23. Snyder, G. J.; Toberer, E. S. *Nat Mater* **2008**, *2*, 105-114.

24. Weiling, L.; Shantung, T. U. *Chin Sci Bull* **2004**, *12*, 1212-1219.

25. Nolas, G. S. *Thermoelectrics: Basic Principles and New Materials Developments;* Springer: Berlin ; New York, 2001.

26. Rowe, D. M. *Int. J. Innov. Energy Syst. Power* **2006**, *1*, 13-23.

27. Tritt, T. M.; Subramanian, M. A. *MRS Bull* **2006**, *03*, 188-198.

28. Winder, E. J.; Ellis, A. B.; Lisensky, G. C. *J. Chem. Educ.* **1996**, *10*, 940.

29. Yan, H.; Sada, N.; Toshima, N. *J. Therm. Anal. Calorim.* **2002**, *3*, 881-887.

30. Feng, X. J.; Xu, J. K.; Lu, B. Y.; Xie, Y.; Huang, R. J.; Li, L. F. *Chin. Phys. Lett.* **2008**, *6*, 2202-2205.

31. Guenes, S.; Neugebauer, H.; Sariciftci, N. S. *ChemInform* **2007**, *31*.

32. Coakley, K. M.; Mcgehee, M. D. *D. Chem. Mater.* **2004**, *23*, 4533-4542.

33. Blouin, N.; Michaud, A.; Leclerc, M. *Adv Mater* **2007**, *17*, 2295-2300.

34. Kulkarni, A. P.; Tonzola, C. J.; Babel, A.; Jenekhe, S. A. *A. Chem. Mater.* **2004**, *23*, 4556-4573.

35. Burroughes, J. H.; Bradley, D. D. C.; Brown, A. R.; Marks, R. N.; Mackay, K.; Friend, R. H.; Burn, P. L.; Holmes, A. B. *Nature* **1990**, *6299*, 352.

36. Wang, L.; Yoon, M. H.; Facchetti, A.; Marks, T. *Adv Mater* **2007**, *20*, 3252-3256.

37. Zaumseil, J.; Sirringhaus, H. *Chem. Rev.* **2007**, *107*, 1296-1323.

38. Ho, H. A.; Bera-Aberem, M.; Leclerc, M. *Chem. Eur. J.* **2005**, *6*, 1718-1724.

39. Park, Y. W. *Synth. Met.* **1991**, *2*, 173-182.

40. Zuzok, R.; Kaiser, A. B.; Pukacki, W.; Roth, S. *J. Chem. Phys.* **1991**, *2*, 1270.

41. Kemp, N. T.; Kaiser, A. B.; Liu, C. J.; Chapman, B.; Mercier, O.; Carr, A. M.; Trodahl, H. J.; Buckley, R. G.; Partridge, A. C.; Lee, J. Y.; Kim, C. Y.; Bartl, A.; Dunsch, L.; Smith, W. T.; Shapiro, J. S. *J. Polym. Sci. Part B: Polym. Phys.* **1999**, *9*, 953-960.

42. Mateeva, N.; Niculescu, H.; Schlenoff, J.; Testardi, L. R. *J. Appl. Phys.* **1998**, *6*, 3111-3117.

43. Toshima, N. *Macromol. Symp.* **2002**, 81-86.

44. Yan, H.; Sada, N.; Toshima, N. *J. Therm. Anal. Calorim.* **2002**, *3*, 881-887.

45. Masubuchi, S.; Kazama, S.; Mizoguchi, K.; Honda, M.; Kume, K.; Matsushita, R.; Matsuyama, T. *Synth. Met.* **1993**, *2-3*, 4962-4967.

46. Österholm, J. E.; Passiniemi, P.; Isotalo, H.; Stubb, H. *Synth. Met.* **1987**, *1*, 213-218.

47. Lévesque, I.; Bertrand, P.; Blouin, N.; Leclerc, M.; Zecchin, S.; Zotti, G.; Ratcliffe, C. I.; Klug, D. D.; Gao, X.; Gao, F.; Tse, J. S. *Chem. Mater.* **2007**, *8*, 2128-2138.

48. Kerileng, M. M.; Peter, M. N.; Rachel, F. A.; Gcineka, M.; Stephen, M. M.; Njagi, N.; Milua, M.; Priscilla, B.; Emmanuel, I. I. *Int. J. Electrochem. Sci.* **2012**, *7*, 11859-11875.

49. Orton, J. W. *The Story of Semiconductors;* Oxford University Press: New York, 2004; pp 510.

50. Atkins, P. W.; Paula, J. D. *Physical Chemistry;* W.H. Freeman: New York, 2006; pp 1053.

51. Heeger, A. J. *Synth. Met.* **2001**, *1*, 23-42.

52. Soderberg, T. *UC Davis Chem. Wiki. , Section 4.3A,* (accessed February 24th, 2014).

53. Bott, A. *Curr. Sep.* **1998**, *17*, 87-91.

54. Skotheim, T. A.; Elsenbaumer, R. L.; Reynolds, J. R. *Handbook of Conducting Polymers;* United States Defense Technical Information Center: 1995.

55. Yue, R.; Yue, J. *Synth. Met.* **2012**, *11-12*, 912-917.

56. Pandey, G. P.; Rastogi, A. C. *Electrochim. Acta* **2013**, *0*, 158-168.

57. Fehse, K.; Walzer, K.; Leo, K.; Lövenich, W.; Elschner, A. *Adv Mater* **2007**, *3*, 441-444.

58. Aleshin, A. *Adv Mater* **2006**, *18(1)*, 17-27.

59. Groenendaal, L.; Jonas, F.; Freitag, D.; Pielartzik, H.; Reynolds, J. R. *Adv Mater* **2000**, *7*, 481-494.

60. Bubnova, O.; Khan, Z. U.; Malti, A.; Braun, S.; Fahlman, M.; Berggren, M.; Crispin, X. *Nat Mater* **2011**, *6*, 429-433.

61. Blanchard, P.; Huchet, L.; Levillain, E.; Roncali, J. *Electrochem. Commun.* **2000**, *1*, 1-5.

62. Hulvat, J. F. Nanoscale Templating and Self-Assembly of Organic Semiconductors, Northwestern University, Evanston, Illinois, 2004.

63. Pei, Q.; Zuccarello, G.; Ahlskog, M.; Inganäs, O. *Polymer* **1994**, *7*, 1347-1351.

64. Du, X.; Wang, Z. *Electrochim. Acta* **2003**, *12*, 1713-1717.

65. Ghosh, S.; Inganäs, O. *Synth. Met.* **1999**, *1*, 413-416.

66. Ouyang, J.; Xu, Q.; Chu, C.; Yang, Y.; Li, G.; Shinar, J. *Polymer* **2004**, *25*, 8443-8450.

67. Zhang, F.; Petr, A.; Dunsch, L. *Appl. Phys. Lett.* **2003**, *25*, 4587.

68. Zotti, G.; Zecchin, S.; Schiavon, G.; Louwet, F.; Groenendaal, L.; Crispin, X.; Osikowicz, W.; Salaneck, W.; Fahlman, M. *Macromolecules* **2003**, *9*, 3337-3344.

69. Kim, D. Segregated Network Polymer-Carbon Nanotubes Composites for Thermoelectrics, Texas A&M University, College Station, TX, 2009.